NIST GCR 11-953

Wildfire Modeling

National Institute of
Standards and Technology
U.S. Department of Commerce

NIST GCR 11-953

Wildfire Modeling

Steven K. Krueger
Department of Atmospheric Sciences
University of Utah
135 S. 1460 E., Rm. 819
Salt Lake City, UT 84112-0110

Grant 60NANB7D6144

November 2011

U.S. Department of Commerce
John E. Bryson, Secretary

National Institute of Standards and Technology
Patrick D. Gallagher, Under Secretary of Commerce for Standards and Technology and Director

Notice

This report was prepared for the Engineering Laboratory of the National Institute of Standards and Technology under Grant number 60NANB7D6144. The statement and conclusions contained in this report are those of the authors and do not necessarily reflect the views of the National Institute of Standards and Technology or the Engineering Laboratory.

NIST 8/15/2007 to 8/14/2011
WILDFIRE MODELING
P.I. Steven K. Krueger

Summary of Accomplishments

No graduate students were supported by the grant; support went to Postdoctoral Fellow - Researcher Dr. Adam Kochanski who joined the project in July 2008. A list of papers and presentations, workshops and seminars, fully or partially supported by the grant is included. Also appended are manuscripts for Kochanski et al (2011) and Kochanski et al (2011). The first is accepted for publication in the International J. of Wildland Fire, pending minor revisions. The second was submitted for review to the J. of Advances in Modeling Earth Systems. Reviewers requested major revisions. The paper was withdrawn. It has merit to NIST, and should be rewritten and submitted for peer-reviewed publication.

Our accomplishments can be summarized as follows. We have aided the development and testing of the LES (Large Eddy Simulator) version of the WRF (Weather Research and Forecasting) model (Wang et al., 2009) coupled with SFIRE, the wildland surface fire module (Mandel et al., 2008, 2011), to simulate wildland fires. As a result of Dr. Adam Kochanski's work with the WRF-SFIRE, he is recognized as a contributor to model development in the most recent release of the WRF model.

The relevance of this work to NIST's WFDS (WUI [Wildland Urban Interface] Fire Dynamics Simulator; Mell et al 2007) is to evaluate the impact of specified atmospheric conditions, topography, domain configurations, and boundary conditions on coupled atmosphere/wildfire model results. Once ignited, the most important environmental property to wildfire behavior is the evolution of the interaction of the fire plume with the ambient wind. As an operational field model, the WFDS must have access to a real-time forecast of atmospheric boundary layer flow. As an operational field model, the WFDS must be able to simulate atmospheric boundary layer flow in the fire domain.

We have concentrated therefore on evaluating the capabilities of WRF-SFIRE and WFDS (whenever WFDS runs are provided) in these terms. Kochanski et al (2011) used the WRF-SFIRE model to examine the sensitivity of grassfire propagation to vertical wind shear. Kochanski et al (2010) used simple hill-topography to examine the sensitivity of simulated hill-flow to model configurations, inflow, and model boundary conditions.

Our accomplishments can be divided into the following parts. The first two follow from Kochanski et al 2010 and Kochanski et al 2011, respectively. The others are work-in-progress as part of grant 60NANB10D225.

(1) Simulations of the Askervein hill flow

Simulations of topographical flow over the Askervein Hill (Kochanski et al 2010) revealed serious discrepancies between the FDS and two other LES models (the WRF model and University of Utah's LES), both on the windward and the leeward side of the hill. The primary reason for differences between model results and observations is suspected to be due to the flow conditions (i.e., neutral atmosphere, steady flow) applied at the boundaries of the single (hill) domain.

To investigate the role of inlet boundary conditions on the evolution of simulated hill-flow, the WRF preprocessing system was modified to provide new, nested LES configurations. Based on studies by others, it is known that well-developed turbulent flow upstream of the Askevein hill provided the best model agreement with flow measurements. The sensitivity of the WRF modeled hill-flow to turbulent, as opposed to steady, inlet flow was examined using a inner (smaller) hill domain nested within an outer (larger) domain. Two configurations of boundary conditions were tested. In the first, cyclic boundary conditions applied to the outer domain allowed the turbulence generated to the lee of the hill to cycle out and back to the inlet of the outer domain. However the wave motions generated by the hill may not necessarily attenuate before entering the inlet of the inner domain. As a result inflow into the inner domain may contain unrealistically amplified flow and turbulence. In the second configuration, open boundary conditions were used and the size of the outer domain was expanded to allow turbulent flow to develop in the outer domain before entering the inner domain. An additional WRF run with a modified surface roughness was performed to determine if surface drag is responsible for the discrepancies between the modeled and observed Askervein hill flow. We plan as part of grant 60NANB10D225 to attempt matching (single domain) FDS runs to determine if its simulations of the Askervein hill-flow improve.

(2) Idealized simulations examining the impact of vertical wind shear on the propagation of grassfires

Kochanski et al (2011) describes four numerical experiments that examine the influence of vertical shear in the low-level wind on wildfire propagation. Kochanski et al was accepted for publication pending minor revisions, and reviewers commented that "This is a potentially very important topic that should be considered during the development of any future operational wildland fire model." Operational wildfire propagation is predicted using simple (mainly empirical) models whose only wind input is the upstream surface wind. The aims of Kochanski et al (2011) are modest: to demonstrate that the vertical wind structure, not just upstream surface wind, is needed to forecast fire (especially severe and/or erratic) behavior and propagation, and that every operational forecast will have a level of uncertainty. The plan is that Kochanski et al (2011) be the first in a series of papers that we propose to write on the fluid-dynamics of atmosphere/wildfire/plume interactions and how they impact fire behavior. Depending on the vertical structure of the background wind, there are atmospheric wind conditions that are inherently unstable to perturbations (supplied by the fire) in the flow. This is quite possibly the triggering means for so-called "blow-up" fires. If the instability occurs for environmental wind profiles of a certain vertical structure, then it should be possible to predict dangerous wildfire behavior based on measurements and/or forecasts of the background vertical wind profile and on knowledge of which vertical wind profile is likely to act as a trigger.

(3) Idealized simulations of updrafts associated with positive temperature perturbations

Using WRF-SFIRE, we performed a series of idealized numerical experiments of stationary updrafts in no-flow conditions. Each updraft was induced by a warm temperature perturbation (i.e., a warm bubble of air) introduced at some height at or above the ground. The numerical experiments differed depending on the vertical moisture profile used, the height placement of the initial temperature perturbation, and the strength of the initial temperature

perturbation. To understand the differences in evolution in each plume simulation, we computed and compared perturbation pressure fields to the horizontal and vertical velocity components of each buoyant warm air bubble. Since numerical experiments of this type are text-book examples (e.g., Markowski and Richardson 2010), we were able to determine that our warm bubble experiments are at least qualitatively similar to the text-book examples and that the pressure fields are calculated correctly. We plan as part of grant 60NANB10D225 to attempt matching FDS runs.

(4) Idealized simulations of stationary fires

Using WRF-SFIRE, we performed a series of idealized numerical experiments of stationary circular fires (ranging in radii from 25 to 200 m) in no-flow conditions. We compared the properties of these simulated plumes to those in (3). We wanted to estimate how similar are plumes driven by surface heating to plumes driven by an idealized temperature perturbation suspended at some height above the ground. Heating in a real fire plume is a combination of both. The convection in a fire plume is driven by radiation, and sensible and latent heat released by the surface combustion, and then by additional latent heating as the plume rises and vapor in the plume condenses. We suspect that the current FDS capabilities for initializing atmospheric temperature and moisture profiles are limited. Using WRF-SFIRE and WFDS simulations, we propose to investigate the relative importance of these two effects in terms of the plume dynamics and the fire propagation. We plan as part of grant 60NANB10D225 to apply the same pressure analyses here as were done for (3).

References

Mandel, J., J. Beezley, L. Cobb, and A. Krishnamur, 2008: A wildland fire model with data assimilation. Mathematics and Computers in Simulation, 79(3), 584606.

Mandel, J., J. Beezley, and A. Kochanski, 2011: Coupled atmosphere-wildland fire modeling with WRF 3.3 and SFIRE. Geoscientific Model Development, 4, 120 doi:10.5194/gmd412011.

Markowski, P.M., and Y.P. Richardson, 2010: Mesoscale Meteorology in Midlatitudes. Wiley, 430 pp.

Mell, W., M.A. Jenkins, J. Gould, and P. Cheney, 2007: A Physics–Based Approach to Modeling Grassland Fires. International J. of Wildland Fire, 16, 1–22.

Wang, W., Bruyère, M. Duda, J. Dudhia, H. Gill, J. Lin, J. Michalakes, S. Rizvi, and X. Zhang, 2009: ARW Version 3 Modeling System User's Guide. Technical report, National Center for Atmospheric Research, 310 pp.

Publications & Activities Fully or Partially Supported by Grant

Articles for publication

Jordanov, G., J. Beezley, N. Dobrinkova, A. Kochanski, and J. Mandel, 2011: Simulation by WRF-Fire of the 2009 Harmanli re (Bulgaria). Lecture Notes in Computer Science. Submitted.

Kochanski, A., M.A. Jenkins, R. Sun, S. Krueger, S. Abedi, and J. Charney, 2011: The importance of low-level environmental vertical wind shear to wildfire propagation. Accepted pending minor revisions. International J. of Wildland Fire.

Mandel, J., J.D. Beezley, and A.K. Kochanski, 2011: Coupled atmosphere-wildland fire modeling with WRF-Fire version 3.3. Geoscientic Model Development, 4, 591610, doi:10.5194/gmd-4-591-2011.

Articles to be prepared for publication

Kochanski, A., M.A. Jenkins, S. Krueger, R. McDermott, and W. Mell, 2010: Capabilities of several models used for wildfire spread to simulate flow over Askervein Hill. J. of Advances in Modeling Earth Systems. Withdrawn. Re-work and resubmit for publication.

Conference presentations & proceeding publications:

Jordanov, G., J. Beezley, N. Dobrinkova, A. Kochanski, and J. Mandel, 2011: Simulation by WRF-Fire of the 2009 Harmanli re (Bulgaria). 8th International Conference on Large-Scale Scientic Computations, Sozopol.

Mandel, J., J. Beezley, A. Kochanski, V.Y. Kondratenko, B. Sousedik, 2010: Wildland fire simulation by WRF-Fire. 2010 American Geophysical Union Fall Meeting, San Francisco.

Beezley, J., A. Kochanski, V.Y. Kondratenko, J. Mandel, B. Sousedik, 2010: Simulation of the Meadow Creek fire using WRF-Fire. 2010 American Geophysical Union Fall Meeting, San Francisco.

Jenkins, M.A., A. Kochanski, S. Krueger, W. Mell, and R. McDermott, 2010: The fluid dynamical forces involved in grass fire propagation. 2010 American Geophysical Union Fall Meeting, San Francisco.

Kochanski, A., M.A. Jenkins, S. Krueger, R. McDermott, and W. Mell, 2010: Evaluation of the fire plume dynamics simulated by WRF-fire. 2010 American Geophysical Union Fall Meeting, San Francisco.

Kochanski, A., M. A. Jenkins, and S.K. Krueger, 2010: Wind forecasting in the fire environment. 24th Annual Conference, Advanced Combustion Engineering Research Center, Brigham Young University, Utah.

Jenkins, M.A., A. Kochanski, and S. Krueger, 2010: The importance of wind in the fire environment. 24th Annual Advance Combustion Engineering Research Center Conference, Brigham Young University, Utah.

Kochanski, A., M.A. Jenkins, S. Krueger, R. McDermott, and W. Mell, 2009: Capabilities of current wildfire models when simulating topographical flow. 2009 American Geophysical Union Fall Meeting, San Francisco.

Jenkins, M.A., A. Kochanski, and S. Krueger, 2009: Wildfire modelling of today and into the future, MITACS/GEOIDE Conference on Forest Fire Modelling. Hinton Training Centre, Alberta.

Kochanski, A., M.A. Jenkins, and S.K. Krueger, 2009: Flow over a simple hill and its impact on wind speed, variability, and turbulence. 8th Symposium on Fire and Forest Meteorology, American Meteorological Society, Kalispell, Montana.

Workshop & meeting presentations & invited seminars

Kochanski, A. 2011: Wind Forecasting for Fire Modeling, Seminar, University of San Jose, CA.

Kondratenko, V., J.D. Beezley, A. Kochanski, and J. Mandel, 2011: Ignition from a fire perimeter in WRF-Fire. 12th WRF Users' Workshop. Boulder, CO.

Krueger, S., A. Kochanski, M.A. Jenkins, 2010: Numerical Simulation of Wildfires: From Idealized to Realistic. Dept of Meteorology and Climate Science, Fall 2010 Seminar Series, San Jose State University.

Krueger, S., A. Kochanski, M.A. Jenkins, 2010: Numerical Simulation of Wildfires: From Idealized to Realistic. Atmospheric, Earth, and Energy Division, Atmospheric Seminar Series, Lawrence Livermore National Laborotory.

Kochanski, A., M.A. Jenkins, S. Krueger, R. McDermott, and W. Mell, 2010: Wind forecasting for fire modeling. Building and Fire Research Laboratory Seminar Series, National Institute of Standards and Technology, Gaithersburg, Maryland.

Jenkins, M.A., A. Kochanski, S. Krueger, R. McDermott, and W. Mell, 2010: Testing the current wildfire models for simulating topographical flow and the implications for prediction of up-hill fire spread rates. Workshop on Front propagation in heterogeneous media: mathematical, numerical, and statistical issues in modelling a forest fire front, Banff International Research Station, Banff, Alberta.

Kochanski, A., M.A. Jenkins, and S.K. Krueger, 2009: Fire spread and hill flow. Wildland–Urban Interface Fires Workshop, National Institute of Standards and Technology, Gaithersburg, Maryland.

Kochanski, A., M.A. Jenkins, and S.K. Krueger, 2008: An overview of wildfire modeling from a LES perspective. Fire Weather and Fire Behavior Modeling Workshop, ESRL, Boulder, Colorado.

Jenkins, M.A., and R. Sun, S.K. Krueger, and J.J. Charney, 2008: The sensitivity of simulated grassland fires to variations in low–level environmental vertical wind shear, Seminar, Department of Meteorology, University of Utah,

Multi-scale Modeling of Wildfires 60NANB7D6144

Appended: Capabilities of several models used for wildfire spread to simulate flow over Askervein Hill

by

Adam Kochanski, Mary Ann Jenkins, Steven K. Krueger,
William E. Mell, and Randall J. McDermott

JAMES
JOURNAL OF ADVANCES IN MODELING EARTH SYSTEMS

Capabilities of several models used for wildfire spread to simulate flow over Askervein Hill

Adam Kochanski [1], *Mary Ann Jenkins* [2], *Steven K. Krueger* [1], *William E. Mell* [3] *and Randall J. McDermott* [3]

[1]Atmospheric Sciences Department, University of Utah
[2]Department of Earth and Space Science and Engineering, York University, Toronto, Canada
[3]Fire Research Division. National Institute of Standards and Technology

Manuscript submitted 28 July 2010

We investigated the capabilities of the WRF-fire, UU-LES, WFDS and WindNinja models when simulating flow over the Askervein Hill. All tested models, except for WindNinja, showed very good agreement with the observations on the windward side of the hill, but differed significantly on the leeward side, where the WRF-fire model overestimated the wind speed by up to 4 m/s, and the UU-LES and the WFDS underestimated it by up to 3 m/s. The official operational version (v.2.1) of WindNinja had problems with providing the flow characteristics corresponding to the observations, and showed inadequate wind speed-up across the hill. The temporal wind speed variability was well represented by the UU-LES model, while WRF-fire showed an order of magnitude smaller standard deviation of the wind speed than observed during the Askervein Hill experiment. Additional tests performed with different combinations of boundary conditions and subgrid-scale parameterizations available for WRF-fire showed that none has a strong enough impact on the time-mean wind speed field to explain the observed discrepancies between the models. While changing the boundary conditions from open to cyclic did not affect the time-mean wind speed field noticeably, it did have a big impact on the WRF-simulated temporal wind speed variability, significantly improving the agreement with observations, especially on the windward side of the hill. Comparison of the results from the tested models using different subgrid-scale closures, as well as the results from WRF simulations using different subgrid-scale parameterizations and boundary conditions, suggests that the terrain-following coordinate system used in WRF-fire may be the reason for the lack of flow separation and associated strong eddies observed downstream of the Askervein hill top that lead to significant overestimation of the wind speed in this area.

1. Introduction

Highly variable winds in complex terrain, together with a high dependence of wildfire-spread rate on the slope inclination, make prediction of the fire behavior in sloped terrain very difficult. Fire often spreads faster uphill than on flat terrain. In research and operational forestry communities, enhanced fire-spread rate in the uphill direction is attributed currently to the decreased distance between the fire flame and the unignited fuel ahead of the flame on the tilted fuel bed; more radiative heat energy reaches the same fuel in a tilted fuel bed in comparison to a level fuel bed, which results in more rapid heating of the fuel and therefore a faster rate of spread. What is not commonly attributed to the faster uphill spread-rate is the likely impact on the wildfire of the behavior and magnitude of the wind due to the sloped terrain. A hill or mountain is a source of energy for the flow field. Research by the atmospheric community has shown that for certain topographic and meteorological conditions, the wind accelerates on the upwind side of the hill, reaches peak values just at and over the crest, and then decelerates on the lee side. This behavior in hill flow is likely important or even crucial to fire-spread rate and fire behavior for two reasons. The reaction intensity of a wildfire is roughly proportional to the wind speed cubed so the speed-up of the flow up and over a hill is an important factor that affects wildfire spread (Bessie and Johnson, 1995). The

To whom correspondence should be addressed.
Adam Kochanski, University of Utah Department of Atmospheric Sciences, 135 S 1460 E, Salt Lake City, 84112, Utah
e-mail: adam.kochanski@utah.edu

fluid dynamical properties of hill flow are a direct consequence of the interactions of the topography with the meteorological conditions in the background flow (Ray, 1986).

A prerequisite therefore to accurate prediction of wildfire spread in complex terrain is the capability to realistically render the wind features associated with common topographic and ambient meteorological conditions. This type of flow rendition is only possible with a numerical fluid dynamical modeling approach that explicitly accounts for nonlinear and nonhydrostatic effects, and allows a detailed representation of the atmospheric flow structure. However, the accurate simulation of topographically-induced flow is difficult, primarily due to its nonlinear character that can result in strong interactions between the mean flow and turbulent eddies.

The problem of accurate simulation is further complicated by the existence of many potentially suitable numerical prediction models that differ in significant ways. Many computational fluid dynamics studies have attempted to simulate the flow over a hill using several types of numerical models, each with distinctly different subgrid-scale parameterizations, model-grid setups, and model-domain initializations. These studies have shown that practically every aspect of a numerical simulation can lead to significant differences in the results obtained. Most valuable from an operational prediction perspective is that such studies attempt to compare their modeling results with meteorological observations from field campaigns. One widely-studied and valuable dataset is the Askervein Hill experiment (Taylor and Teunissen, 1985), which consisted of a field campaign that was conducted in 1983 with the purpose of capturing wind data representing hill flow under near-neutral stratification and steady wind conditions. Under these ambient meteorological conditions, the Askervein Hill is as close to ideal for studying steady-state airflow over "small-amplitude" hills. The Askervein Hill experiment is also the best to-date dataset for testing the properties and accuracy of the different numerical models used to simulate this type of flow.

In a comparison of the results from a mass-consistent (kinematic) model and a 3D Navier-Stokes solver with the wind measurements from the Askervein Hill experiment, Lopes (2003) concluded that the observed wind speed-up on the windward side of the hill was represented well by both models. On the leeward side of the hill, the simple mass-consistent kinematic model was not able to correctly reproduce the observed flow deceleration, while the more advanced 3D Navier-Stokes model showed good agreement with the observations. Numerical simulations of the flow over the Askervein Hill performed using a Reynolds-averaged Navier Stokes or RANS approach (Castro et al., 2003) and a Large-Eddy Simulation (LES) model (Lopes et al., 2007) also came to similar conclusions. Both the RANS and LES models represented the flow on the windward side of the hill very well. On the leeward side, however, the RANS k-ε model simulated deceleration of the flow significantly better than the LES, which substantially underestimated the wind speed.

Analyses of the results from numerical simulations with different grid sizes shows that grid refinement also has an impact on the accuracy of the predicted wind speed downstream of the hill top (Lopes et al., 2007), and that higher resolution does not necessarily lead to better results. The non-linear micro-scale simulations performed by Undheim et al. (2006) showed that vertical resolution plays the most important role, while changes in horizontal resolution do not affect the results significantly. Additionally, this study pointed out that the decelerating turbulent flow downstream of the hill top is more sensitive to the changes in the grid setup than is the accelerating upstream flow.

In a LES, a subgrid-scale model is used to model smaller-scale energy-carrying turbulent motions, while larger-scale energy-carrying motion is resolved. The subgrid-scale (SGS) turbulence closure model used in a LES appears to play a significant role in terms of model accuracy as well. For example, the LES utilizing the Dynamic Reconstruction Model (DRM) proposed by Chow and Street (2009) provided better results than the commonly used 1.5-TKE-based SGS closure model. Deploying the higher-order DRM to model SGS turbulence led to a better representation of the deceleration on the leeward side flow and consequently to better agreement with the Askervein Hill wind observations. The study of Chow and Street (2009) suggests that increasing the complexity of the SGS model is beneficial and improves the accuracy of a LES of flow in complex terrain. However, the results from nested LESs presented in a recent study by Golaz et al. (2009) show that the much simpler approach based solely on a first-order Smagorinsky SGS turbulence closure, without any dynamic reconstruction, can also provide results that compare well with the Askervein Hill flow observations.

In summary, many approaches to the problem of accurate simulation of small-scale topographical flows

have been proposed. These differ by model type and complexity, and even though each approach uses a different combination of SGS parameterization, initialization, grid sizes, and boundary conditions, the results are often similar to the observations. All these studies provide insights into the problem of simulating topographical flow and point out key elements that affect the accuracy of topographical flow simulations. They also show that the complexity of the problem does not allow for evaluation of the models based soley on their specifications. It does not seem possible at present to recommend one type of model or one SGS parameterization for providing the best results in all situations. Therefore, the only way to assess how well the current numerical fluid dynamical coupled wildfire-atmosphere models handle topographical flow prediction is to evaluate their results based on the available observations. In this study we analyze the capabilities of four different numerical wildfire-atmosphere models for simulating topographical flow.

2. Methodology

The first model is WRF-fire (Mandel et al. 2008, 2009). This is the coupled wildland fire version of WRF (the Weather Research and Forecasting Model (Wang et al., 2009) WRF is selected for this study due to its completeness as a weather forecasting system that includes one- and two-way domain nesting, and flexible dynamics and physics that can be downscaled to very high resolutions and be used for LES with real atmospheric forcing. These capabilities allow the WRF-fire model to be used to simulate wildfires with idealized but realistic atmospheric forcing, as well as for real-time wildfire forecasting. WRF-fire is the only community model, to the authors' knowledge, that is ready for multiscale atmospheric and wildfire simulation and forecasting using initial and lateral boundary conditions from larger-scale numerical weather prediction models. It is estimated that within two to three years WRF will be able to simulate atmospheric phenomena with spatial scales ranging from several-hundred kilometers to several hundred meters in real-time, with the small-scale turbulent near-surface flow in complex terrain resolved by the LES approach (Liu et al., 2009). The wildfire model coupled with the WRF is user-chosen to be either the Rothermel fire behavior formulation (Rothermel, 1972) or the McArthur formulation (Noble et al., 1980) for fire spread rate. The second model is the University of Utah's Large Eddy Simulation model (UU-LES), which is an advanced research LES model (Zulauf, 2001) coupled with a version of Clark's wildfire model (Sun et al., 2009). The fire model coupled with the UU-LES is again user-selected, and fire spread can be either the Rothermel, McCarther, or the Canadian FBPS (Hirsch, 1996) formulation. The third model is NIST's WFDS (Wildland Urban Interface [WUI] Fire Dynamics Simulator) described by Mell et al. (2007). WFDS is also a LES that, unlike WRF-fire and the coupled wildfire-atmosphere UU-LES, contains the physics for modeling thermally-driven flow and heat transport associated with fire and resolves combustion processes. The last model is WindNinja v.2.1 (Forthofer and Butler, 2007), a mass-consistent model that does not employ the 3D conservation of momentum equations, but instead finds a divergence-free velocity field based on the topography and initial wind field. It is equivalent to the NUATMOS model described by Lopes (2003). The main difference between these two mass-consistent models is that the latter is initialized with wind data from a number of locations and uses the wind profile reconstructed from observations, whereas the former one uses as input the wind speed and direction at one location and one level only. WindNinja is selected for this study because of its great simplicity and computational performance that allows for easy implementation as an atmospheric component driving operational wildfire prediction models like the FARSITE (Finney, 1998). The main features of the four models used in the study are presented in Table 1. The basic differences between the three LES models are the boundary conditions, coordinate systems, and the subgrid-scale parameterization schemes.

To assess the capabilities of these four models when simulating topographical flow, we chose to use measurements from the Askervein Hill Experiment (Taylor and Teunissen, 1985) for model initialization and to compare each model's results with observations. As with previous studies, the Askervein Hill Experiment is chosen because it is still the most comprehensive field experiment devoted to the small-scale topographical flow and therefore the most commonly used dataset for evaluation of model capabilities in complex terrain. As described in Section 1, the Askervein Hill Experiment dataset has been used extensively for validation of various types of atmospheric models, starting with simple mass-consistent models (Lopes, 2003), then RANS models (Castro et al., 2003), and finally LES with explicit filtering and dynamical reconstruction (Chow and Street, 2009). Using the same dataset in this study for the evaluation of the atmospheric components of the four wildfire models is an opportunity for comparison with other previously tested models.

	WRF-fire	UU-LES	WFDS	WindNinja
Type	LES	LES	LES	Mass-consistent
Horizontal boundary conditions	Open /Cyclic	Cyclic	Cyclic	-
Surface boundary conditions	logarithmic	logarithmic	logarithmic	-
Coordinate system	Terrain following (eta)	Cartesian grid	Cartesian grid	-
Subgrid-scale closure	1.5 TKE / Smagorinsky	1.5 TKE	Dynamic Smagorinsky	-
Domain size	260x260x200	256x256x200	128x128x120	256x256
Horizontal domain size	5382 x 5044 m	5300 x 4960 m	2650 x 2480 m	-
Horizontal resolution (Δx, Δy)	20.7 x 19.4 m	20.7 x 19.4 m	20.7 x 19.4	20 x 20 m
Height of the first vertical level	3.7 m	3.0 m	5.0 m	-
Top of the domain	600 m	600 m	600 m	-

Table 1: Comparison of the analyzed models.

The approximately elliptically-shaped Askervein Hill is located on the island of the South Uist (Outer Herbrides of Scotland), and is 116 m high (126 m above the sea level), with a minor axis approximately 2 km and a major axis of 1 km in length. The topography of the hill, together with the domain size of the WRF-fire model and UU-LES, are presented in Figure 1.

The black line, crossing the hill top, denoted by 'A' in this figure, is the measurement line along which meteorological observation towers were installed. From the Askervein Hill Experiment, we selected a subset dataset corresponding to October 3, 1983. This day is considered to be the best measurement day of the entire field campaign, with a relatively steady, strong wind from the 210° direction, blowing approximately perpendicular to the long axis of the hill. For the initialization of the wind field in the Large-Eddy Simulation models, we used the wind profile reconstructed from the tower measurements for the first 30 m above ground level (AGL), kite measurements up to 384 m AGL, and rawinsonde measurements taken at the reference station located roughly 4 km upstream of the hill top. The temperature and moisture fields in WRF-fire and UU-LES models were initialized using the rawinsonde temperature and moisture profiles taken at the same location, whereas WFDS used a constant temperature lapse rate of 10K/km. The atmospheric profiles used for the initialization of these LES models are presented in Fig. 2. The vertical profiles in this figure show that, for the analyzed day, the atmosphere was slightly unstable up to 90 m AGL and stable aloft, with a very moist layer extending from the surface to 1400 m AGL. The mean wind direction was 210° (approximately south-westerly). The WindNinja was initialized using the wind speed and direction measured at the reference station (4 km south-east from the hill top) at 10 m AGL. WindNinja's user interface of the current operational version (2.1) does not allow for initialization with a specified wind profile.

3. Results

Many previous numerical studies based on the Askervein Hill Experiment have shown that it is difficult task for the numerical models to reproduce correctly the changes in the wind speed along the measurement line 'A' indicated in Fig. 1 (see Lopes (2003), Castro et al. (2003), Undheim et al. (2006), Silva Lopes et al. (2007), Chow and Street (2009)). Significant flow acceleration occurs on the windward side of the hill as the flow approaches the hill top, while on the leeward side of the hill, rapid deceleration is observed. Turbulent flow develops, with very strong eddies, on the leeward side of the hill, and this is the place where the most significant discrepancies between modeled wind results and observed flow occur. Therefore, in this study, we focus on the wind measurements taken along this line and use this wind data to compare to and to evaluate the results of the four models (see Fig. 3).

All of the Large-Eddy Simulation models produced flows that, on the windward side of the hill, match the observations (blue solid line) very well. There is significant speed-up as the flow reaches the hill top. The maximum wind speed simulated by the LES models does not differ from the measured wind speed by more than 10%. The

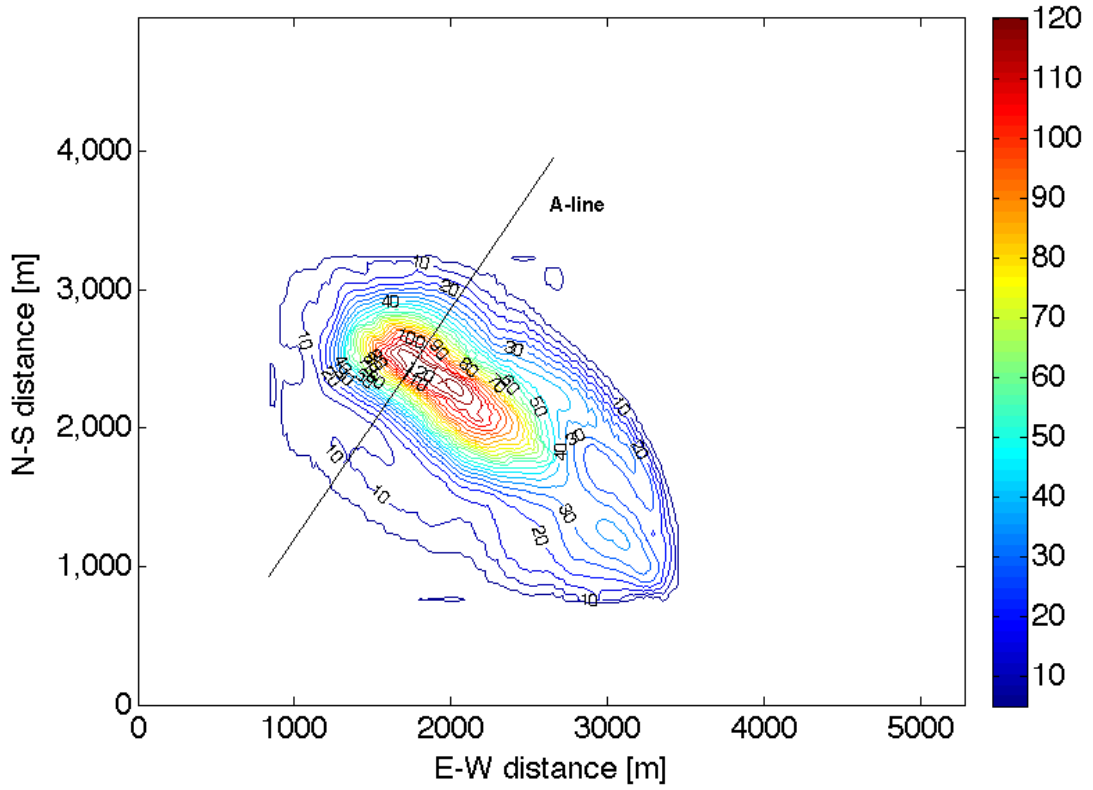

Figure 1: Topography of the Askervein hill with the location of measurement line 'A'.

biggest differences between the simulated and measured wind speeds occur on the leeward side of the hill. Here none of the models simulate the observed flow deceleration particularly well. Over the first 100 m north-east of the hill top, the WRF captures the wind speed decrease very well. However, past that point, further downstream of the hill top, the wind speed is overestimated by up to 4 m/s in the WRF simulation. The opposite is true for UU-LES and WFDS models. They reproduce successfully the flow speed-up on the windward side of the hill but fail to reproduce correctly the flow slow-down downstream of the hill top. Both models show too rapid a flow deceleration — underestimating the wind speed by up to 1.5 m/s — compared to observations. The only model that was not able to capture either the observed wind speed-up on the windward side of the hill or at its top is WindNinja. The performance of WindNinja seems to be significantly worse than kinematic models analyzed by Lopes (2003) and Forthofer and Butler (2007).

The main reason for WindNinja not capturing the observed flow is that the official (operational) version v. 2.1 does not allow input of the actual wind profile for initialization. Instead, based on a wind speed at a certain height and the surface type characterizing its roughness, the model constructs a logarithmic vertical wind profile. Changing the vertical wind profile initialization in WindNinja v 2.1 to allow the use of the actual wind profile improves model performance, bringing it much closer to the wind results from the more advanced LES models and to observations (Forthofer (2007)). The sensitivity of WindNinja to the input wind profile implies that the wind shear in the initial profile is crucial for a correct representation of the flow speed-up across the hill. The maximum wind speed at the hill top simulated by WindNinja seems to correspond exactly to the initial wind speed. Therefore, the initial underestimation of the wind speed aloft, due to the reconstruction of the wind speed based on the measurement at one level, limits the wind speed maxi-

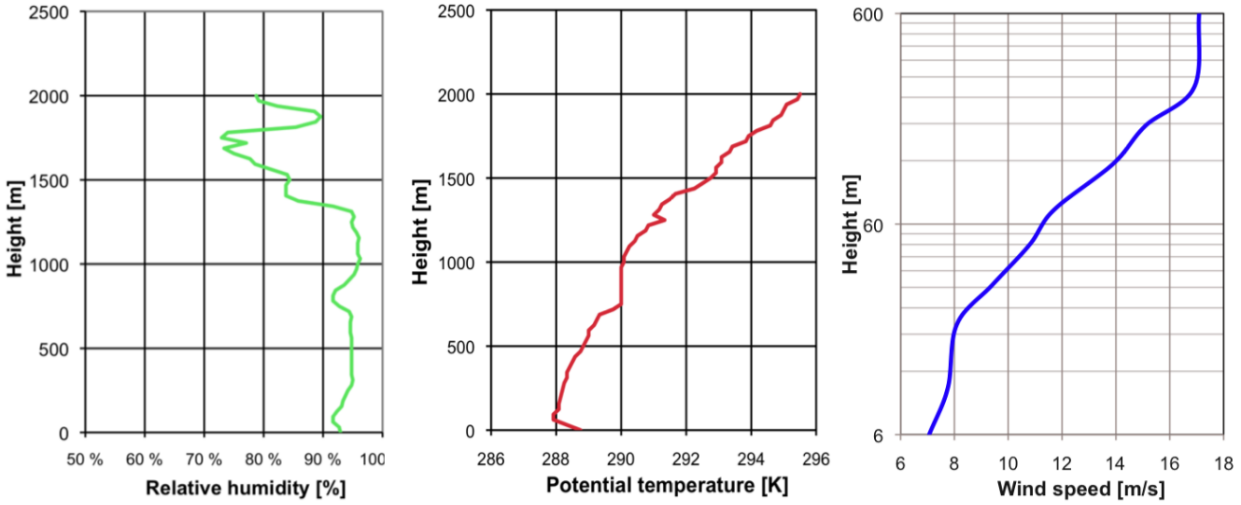

Figure 2: The atmospheric profiles of relative humidity, potential temperature and wind speed measured at the reference station on October 3, 1983, and used for model initialization.

mum at hill top as shown in Fig. 3.

The reasons for the biases between the time-averaged wind speeds of the LES models and the field measurements are less straightforward. The comparison of the mean wind speed fields at 10 m AGL simulated by WRF-fire, UU-LES, and WFDS shows that the agreement between the model results is not limited to the 'A' measurement line only (see Fig.4). In fact, the flow over the whole windward (south-west) side of the hill is equally well captured by the LES models. Each LES shows a slight deceleration of the flow between 800 and 400 m upstream of the hill top, followed by a rapid acceleration on the windward sloped part of the domain (starting roughly 400 m ahead of the hill top). This windward-side flow behavior seems to be universal since it is observed for all cross-sections through the hill parallel to the measurement line 'A' (see Fig.4).

The only model that does not agree with this wind pattern is the WindNinja. As discussed previously, due to the model's restricted initialization, the range of wind speed simulated by WindNinja is limited and WindNinja does not produce an adequate windward-side speed-up.

The leeward side of the hill is the area over which the LES models show the biggest biases with respect to the observations. Compared to the wind speed observed along the 'A' line on this side of the hill, UU-LES and WFDS winds rapidly decelerate leading to a wind speed drop to 3-6 m/s, whereas WRF-simulated wind speed drops only to 8-10 m/s. Statistics of the model performance along the 'A' line are presented in Table 2. As listed the WRF-fire wind has the best correlation with the measurements as well as the smallest Mean Absolute Error. However, UU-LES and WFDS models exhibit comparable statistics even though their flow characteristics downstream of the hill are quite different. Unlike the flow behavior on the windward side of the hill, cross-hill wind profiles on the leeward side change as we move southeast from the 'A' line. The most pronounced flow deceleration is simulated by UU-LES and WFDS. It is located roughly around the 'A' line, and extends southeast one third of the hill's length. Cross-sections located southeast from the 'A' line show less pronounced flow decelerations for the southeast half of the hill lee-side, all models show a similar moderate reduction in wind speed. As a consequence of the location of this deceleration zone in UU-LES and WFDS simulations, their results differ much more from measured winds along the 'A' line than they do southeast from it. For this reason the measurement line seems to be the best suited for examination of differences between the models.

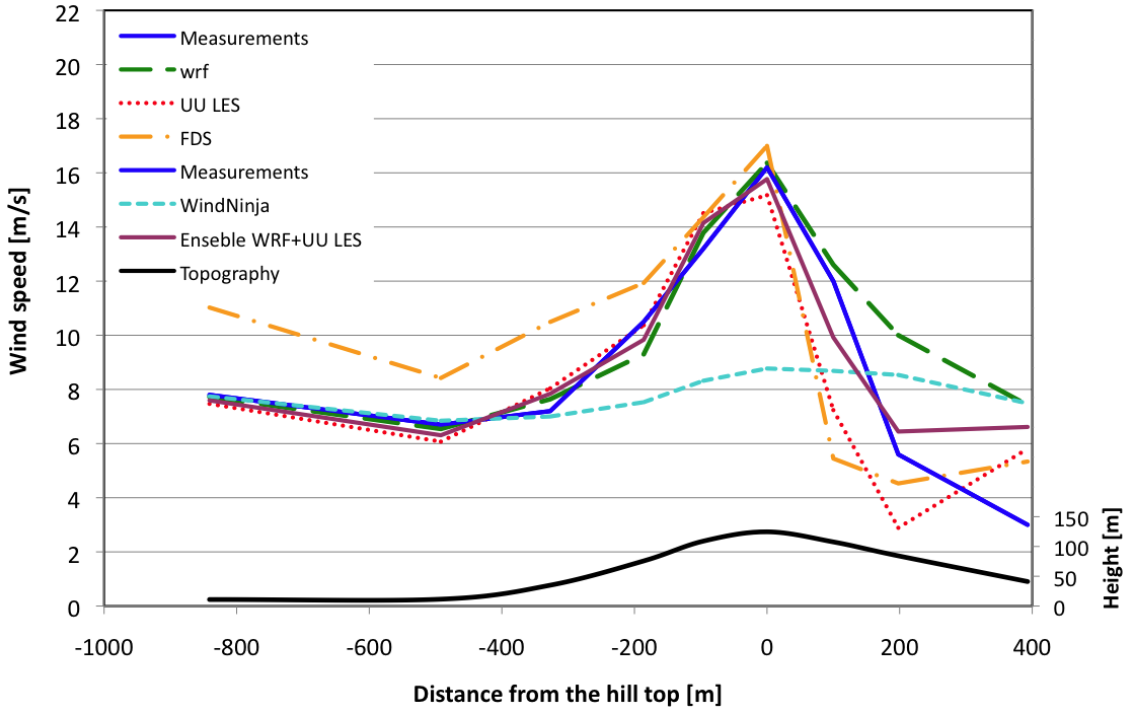

Figure 3: Measured and simulated time-averaged wind speeds at 10 m AGL across the hill, along the 'A' line. The black line and the right axis represent the topography of the hill in the 'A' direction.

	WRF-fire	UU-LES	WFDS	WindNinja
correlation coefficient (R)	0.88	0.85	0.74	0.6
Mean Absolute Error	1.34 m/s	1.62 m/s	2.07 m/s	2.93 m/s

Table 2: Statistical comparison between the 10 m wind speed simulated and measured along the 'A' line.

In addition to the average wind speed, temporal variability in the wind is also very important for wildfire prediction. Strong fluctuations in wind speed may cause erratic wildfire behavior that significantly increases the risk associated with wildfire fighting operations. Fig. 5 a) shows the standard deviations of the 10 m AGL wind speed of the measured winds and the WRF-fire and UU-LES simulated winds along the 'A' line. The observed standard deviation was computed from 1 Hz low-pass filtered Gill anemometer data, digitized to 2 Hz (see Taylor and Teunissen, 1985). The simulated wind speed standard deviations were computed from the model output saved at 10 s intervals. The temporal wind speed fluctuations stay at an almost constant level upstream of the hill top, then increase sharply at the hill top, and then decrease slightly downstream of it. This variation in wind speed was best captured by UU-LES, with a slight overestimation compared to observed values and an onset of peak values roughly 200 m ahead of the peak in observed values. The WRF-fire model, on the other hand, was not able to reproduce the observed temporal variations in the wind speed across the hill. For this model the temporal wind speed fluctuations stay at an almost constant level upstream and downstream of the hill top.

4. Reasons for the discrepancies between the models.

The most striking features apparent in Figs. 3 and 4 are the similarity of the model results for the windward side of the hill, where all LES-type models performed well, and the significant discrepancies on the leeward side of

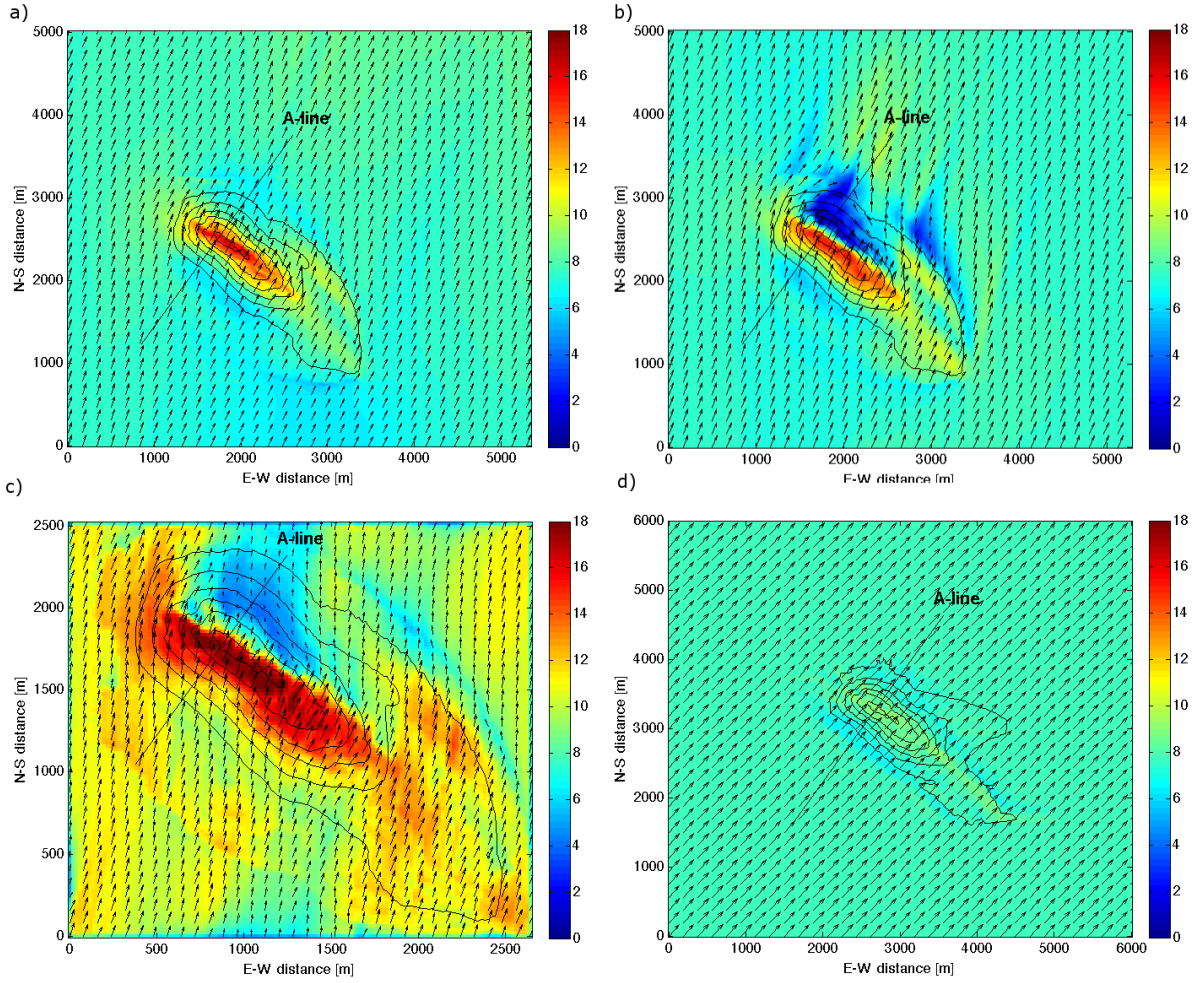

Figure 4: *X-y* cross sections of time-averaged wind speed at 10 m AGL as simulated by: a) WRF-fire, b) UU-LES, c) WFDS, and d) WindNinja. Black contour lines represent topography and the vectors (every 8th grid point shwn) denote flow direction in the *x-y* plane, color fill represents wind speed [m/s].

the hill, where all models had problems simulating flow deceleration. A closer look at the Fig. 5 b) and Fig. 4 b) reveals that the region of the rapid flow deceleration corresponds exactly to the area of the strongest temporal variations in the wind speed. This suggests that the strong reduction in the wind speed downstream of the hill top is a result of the strong eddies formed on the leeward hill side. To determine the strength of these eddies, the vertical vorticity field,

$$\zeta = \widehat{k} \cdot (\nabla \times \overrightarrow{V}) = \frac{\partial v}{\partial x} - \frac{\partial u}{\partial y}$$

is computed from the mean wind field at 3 m AGL. Here u and v are the east-west (x direction) and north-south (y direction) wind components. An overlay of the mean vorticity and the instantaneous wind vector at first model level (3 m AGL) confirms that the region of the strongest flow deceleration contains two persistent eddies indicated by the distinctive minima and maxima in the mean vorticity field (see Fig.6 a).

Note that these two eddies, located symmetrically on both sides of the measurement line, induce reversed flow indicating separation of the surface flow from the flow aloft in the area downstream of the hill top. WRF-fire results show neither persistent eddies in this area nor any

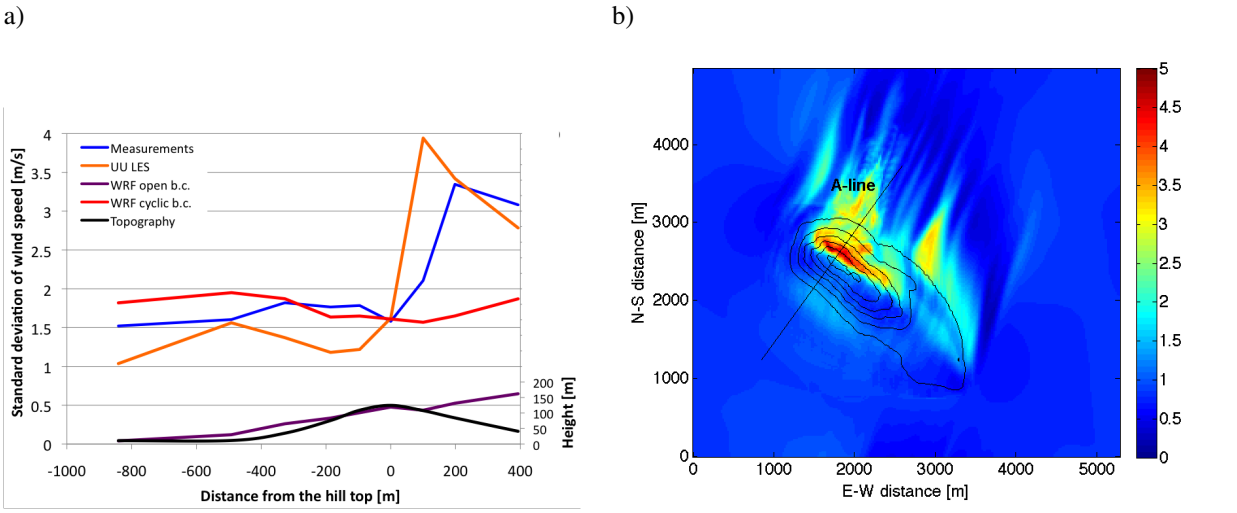

Figure 5: Standard deviation of the wind speed at 10 m AGL from the time mean : a) for the simulated and observed winds along measurement line 'A' (The black line and the right axis represent the topography of the hill in the 'A' direction). ; b) and the spatial distribution based on UU-LES modeled winds (black contour lines represent topography).

indication of flow separation. Contrary to UU-LES simulations, the flow simulated by WRF-fire exhibits strong vorticity mostly on the hill top, with very small values on the leeward side of the hill where UU-LES predicts strong eddies. UU-LES shows permanent flow separation in the area where WRF-fire shows none. Observations from the Askervein Hill experiment confirm the existence of the intermittent flow separation below 10m AGL in this area. This difference in the way the models simulate the flow in the unsteady zone behind the hill top explains the discrepancies between their results in terms of the flow deceleration downstream of the hill top. It also explains why the ensemble average of these two models shows the best performance among the four models, with a correlation coefficient R=0.93 and a Mean Absolute Error of 1.09 m/s with respect to observations.

The LES-type models differ in terms of coordinate systems, subgrid-scale parameterizations, and boundary conditions. We try here to determine how these differences affect model results. There are several possible reasons for the observed discrepancies between the measurements and UU-LES, WFDS and WRF-fire results. Among these three models, only WRF-fire allows for an easy change of both the subgrid-scale parameterization scheme and boundary conditions. Therefore, we can use WRF-fire to investigate the impact of these factors.

As discussed in the previous section, the standard deviations of WRF-simulated wind speed at 10 m AGL (violet line on Fig. 5a) are significantly lower than the ones derived from either the measurements or UU-LES and WFDS simulations. The observed, almost linear increase, in the standard deviations of WRF-simulated wind speed in the downstream direction may indicate turbulence suppression due to the lateral boundary conditions. The open boundary condition, unlike the cyclic one used in UU-LES, does not allow for turbulence recirculation. As a consequence, the turbulence must be generated within the model domain, since no eddies are present at the open inflow boundary. This situation could lead to the slow linear increase in the temporal wind speed variability shown by the purple line in Fig. 5 a). Since WRF-fire is the only model run with open boundary conditions, it is reasonable to assume that open boundary conditions are responsible for there being no turbulence at the inflow boundaries, leading to less turbulent flow in the interior of the domain, and consequently a lower temporal wind speed variability downstream. To test this hypothesis, we performed an additional WRF-fire run with a similar model configuration as in the original case, but with cyclic, instead of open, boundary conditions. The results presented in Fig. 5 a) show that in fact the temporal wind speed variability increased after employing cyclic boundary conditions. The standard deviations of the wind speed sim-

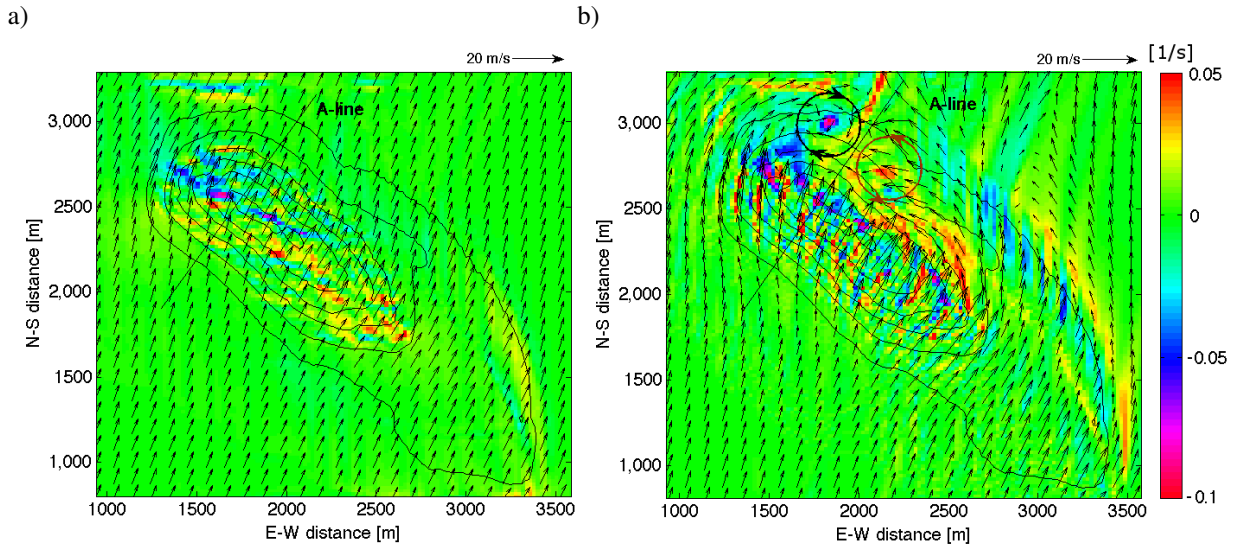

Figure 6: Time-averaged vorticity field [1/s] in the first model level and snapshot of the wind field at the same level simulated by: a) WRF-fire and b) UU-LES. Black and brown circles indicate regions of strong negative and positive vorticity, respectively, corresponding to the presence of the anticyclonic and cyclonic eddies evident on the overlaid wind vector field. Vectors (every 5th grid point shown) denote instantaneous flow in the *x*-*y* plane, contour lines represent topography.

ulated using cyclic boundary conditions are now in reasonable agreement with observations on the windward side of the hill. However, downstream from the hill top, the temporal wind speed variability is still significantly underestimated. It seems that the temporal wind speed fluctuations upstream of the hill top, where the flow is not very turbulent, are captured significantly better if the domain boundaries allow constantly evolving turbulent flow to pass through the domain boundaries. Chow and Street (2009) report that simulations using a constant inflow or a constant inflow with random perturbations did not give satisfactory results with their LES DRM formulation. To provide a realistic turbulent inflow, inherently unsteady turbulent flow throughout their model domain, and satisfactory agreement with Askervein wind measurements, Chow and Street performed a separate neutral boundary-layer simulation with periodic boundary conditions, geostrophic forcing, and flat terrain, and data extracted from a slice in the domain at every time step were then used to specify the model's inflow velocity at every time step on the inflow side of the Askervein domain.

However, cyclic boundary conditions do not solve the problem in WRF-fire of the wind speed and variability underestimation downstream of the hill top, where wind speed simulated with open boundary conditions was very similar to that simulated with cyclic boundary conditions. On average, the wind speed along the 'A' line simulated with cyclic boundary conditions was 0.15 m/s greater than the one with open boundary conditions. As a consequence, the run with periodic boundaries showed an even greater overestimation of the wind speed downstream of the hill top compared to the one with open boundaries.

Another factor that may be responsible for the discrepancies between the LES model results and the observations is the type of subgrid-scale closure used by each model. Chow and Street (2009) show implementing of more advanced subgrid-closure techniques (i.e., their DRM) may significantly improve model results, especially downstream from the hill top where the discrepancies between model results and observations are the most pronounced. The results in this study suggest something different. The UU-LES and WFDS, even though based on different subgrid-scale parameterizations (1.5 TKE versus first-order Smagorinsky, respectively), showed similar results with substantial underestimation of the wind speed on the leeward side of the hill. We investigated the effect of the subgrid-scale closure by

running a WRF-fire simulation with the same setup as the original one presented in Table 1, but with a Smagorinsky, instead of the 1.5 TKE, closure model. The results from this run were essentially identical to the original run with the 1.5 TKE closure, and the wind speed from the "Smagorinsky" run was only around 0.3 m/s smaller than the original run. The reason for that is probably significantly higher horizontal and vertical resolution of investigated models than the one used by Chow and Street (2009). In our study the first WRF vertical level was situated at 3.7 m above the ground, and the horizontal resolution was approximately 20m, while most of the runs investigated by Chow and Street were set up with 32 m horizontal and 10 m vertical resolution. Higher resolution of our model, makes it probably less sensible to the subgrid-scale paramterization, as wider range of small scales gets explicitly resolved. That may explain small differences between the runs based on different subgrid-scale schemes.

With different subgrid-scale closure models, UU-LES and WFDS also have similar flow characteristics, with very rapid deceleration and turbulent eddies formed downstream of the hill top. This result, together with the very similar results from WRF-fire simulations performed with the 1.5 TKE and Smagorinsky subgrid-scale parameterizations, supports the thesis that, in this case at least, the subgrid-scale parameterizations do not play a key role and are not responsible for the observed discrepancies among the models. Since neither boundary conditions nor the subgrid-scale parameterizations significantly affected the mean wind speed the model coordinate system seems to be the most probable reason for the observed inconsistencies between WRF-fire, UU-LES, and WFDS. Unfortunately, none of these models allows for a change in the coordinate system, so we cannot perform an experiment that directly shows its effect on the results of the flow simulation over the hill. However, there are other studies confirming that the terrain-following coordinate system (as used in WRF-fire), may significantly affect the results in cases of a flow over a complex terrain. Lundquist et al. (2010) showed that truncation errors — the result of using a terrain-following coordinate system in complex terrain — can have a significant impact on the prediction of wind, and the advection and concentration of a scalar field. The idealized simulations performed by Lundquist et al. (2010) using WRF with the terrain-following coordinate system and with the Cartesian grid with immersed boundary method, showed (their Figure 3) that in a case of flow across complex terrain the truncation errors lead to artificial flow accelerations downstream an orographic obstacle The numerical simulations of the flow over an isolated hill performed by Ohba et al. (2002) also confirmed that the type of coordinate system does impact the characteristics of the flow downstream of the hill top. The streaklines simulated by the model with a body-fitting (terrain-following) grid were significantly less complex than the ones simulated by the same model but with orthogonal Cartesian coordinates. Additionally, the most pronounced differences between the results from models with Cartesian and with terrain-following grids were apparent on the leeward side of the hill. Here the "orthogonal" model showed very evident flow separation, while the model with terrain-following coordinate system showed none (see Ohba et al. 2002, Figure 17). Since these conclusions are consistent with our observations, the terrain-following coordinate system used by WRF-fire appears to be the main reason for the discrepancies observed downstream of the hill top. The inadequate representation of the downstream eddies, and the lack of reversed flow and flow separation on the lee of the hill, seem to produce the overestimation of the wind speed in WRF simulations. On the other hand, intense turbulent eddies and a persistent flow separation downstream of the hill top lead to overly rapid flow deceleration and an underestimation of the leeward-side wind speed by UU-LES and WFDS models.

5. Conclusions

The results from WRF-fire, UU-LES, WFDS and WindNinja show that all of these models have some deficiencies when applied to the simulation of hill flow. The operational version 2.1 of WindNinja that is initialized with a one-level upstream wind speed is not capable of realistic simulation of the flow over the Askervein hill. The wind speed at the hill top simulated by this mass-consistent model is only about half the observed wind speed and that simulated by the LES-type models. Note that even though the official current operational version of the WindNinja performs poorly in the Askervein Hill case, this should not be taken as a general result for mass consistent models. In fact the same model — but initialized with the full wind profile — performed comparably to the tested LES-type models (Forthofer, personal communication). All LES-type models showed very good agreement with the observations on the windward side of the hill, but differed significantly from observa-

tions on the leeward side. Here WRF-fire overestimated the mean wind speed by up to 40%, and UU-LES and WFDS underestimated it by up to 50%. The temporal wind speed variability was well represented by UU-LES, while WRF-fire with open boundary conditions showed an order of magnitude smaller standard deviation in the wind speed than observed. Changing the boundary conditions in WRF-fire from open to cyclic increased the temporal wind speed variability on the windward side of the hill to a level in close agreement with observations. The significant increase in the wind speed variability downstream of themodels hill top — evident in UU-LES results and observed during the field study — was not captured correctly by WRF-fire even with open boundary conditions. The time-averaged vorticity fields from UU-LES and WRF-fire show that WRF-fire does not capture correctly the eddies that formed downstream of the hill. Their absence does not allow for correct simulation of the flow deceleration, and as a consequence the WRF-predicted mean wind speed is significantly overestimated on the leeward side of the hill. The two tests performed with WRF-fire , each using a different subgrid-scale parameterization (1.5 TKE versus Smagorinsky), excluded the choice of subgrid-scale closure as the factor primarily responsible for the model discrepancies and disagreement with observations downstream of the hill top. Only the coordinate systems (terrain-following versus Cartesian) appear responsible for the differences in the lee flow results between WRF-fire and other LES. This conclusion is based on the recent study by Lundquist et al. (2010) and numerical experiments performed by Ohba et al. (2002). Nevertheless, only additional experiments performed with the future version of WRF based on the Cartesian grid (not available yet) would allow for further verification of this conclusion.

Acknowledgments

This research was supported by Department of Commerce, National Institute of Standards and Technology (NIST), Fire Research Grants Program, Grant 60NANB7D6144. A grant of computer time from the Center for High Performance Computing, University of Utah, is gratefully acknowledged.

References

Bessie, W. C. and E. A. Johnson, 1995: The relative importnace of fuels and weather on fire behavior in subalpine forests. *Ecologgy*, **76 (3)**, 747–762.

Castro, F., J. Palma, and A. S. Lopes, 2003: Simulation of the askervein flow. part 1: Reynolds averaged navier–stokes equations (k-ε turbulence model). *Boundary-Layer Meteorol*, **107 (3)**, 501–530.

Chow, F. K. and R. L. Street, 2009: Evaluation of turbulence closure models for large-eddy simulation over complex terrain: flow over askervein hill. *J. Appl. Meteor. Climatol*, **48**, 1050–1065.

Finney, M., 1998: Farsite: Fire area simulator—model development and evaluation. *Res. Pap. RMRS-RP-4*, 1–47.

Forthofer, J. and B. Butler, 2007: Differences in simulated fire spread over askervein hill using two advanced wind models and a traditional uniform wind field. *USDA Forest Service Proceedings*, **RMRS-P-46**.

Forthofer, J. M., 2007: Modeling wind in complex terrain for use in fire spread prediction. *PhD thesis, Colorado State University, Fort Collins, CO*, 1–123.

Golaz, J.-C., J. D. Doyle, and S. Wang, 2009: One-way nested large-eddy simulation over the askervein hill. *Journal of Advances in Modeling Earth Systems - Discussion*, 1–4.

Hirsch, H. K., 1996: Canadian forest fire behavior prediction (fbp) system: user's guide. *Special Report*, **7**.

Liu, Y., Y. Y. L. Liu, W. Cheng, W. Wu, T. T. Warner, and K. Parks, 2009: Simulating intra-farm wind variations with wrf-rtfdda-les. *10th WRF Users Workshop, NCAR*, 1–19.

Lopes, A. M. G., 2003: Windstation—a software for the simulation of atmospheric flows over complex topography. *Environmental Modelling & Software*, **18**, 81–96.

Lopes, A. S., J. Palma, and F. A. Castro, 2007: Simulation of the askervein flow. part 2: Large-eddy simulations. *Boundary-Layer Meteorol*, **125 (1)**, 85–108.

Lundquist, K., F. Chow, and J. Lundquist, 2010: An immersed boundary method for the weather research and forecasting model. *Monthly Weather Review*, doi: 10.1175/2009MWR2990.1.

Mandel, J., J. Beezley, J. Coen, and M. Kim, 2009: Data assimilation for wildland fires. *Control Systems Magazine*, **29 (3)**, 47–65, doi:10.1109/MCS.2009.932224.

Mandel, J., L. Bennethum, J. Beezley, J. Coen, C. Douglas, M. Kim, and A. Vodacek, 2008: A wildland fire model with data assimilation. *Mathematics and Computers in Simulation*, **79 (3)**, 584–606.

Mell, W., M. Jenkins, J. Gould, and P. Cheney, 2007: A physics-based approach to modelling grassland fires. *International Journal of Wildland Fire*, **16 (1)**, 1.

Noble, I. R., A. M. Gill, and G. A. V. Bary, 1980: Mcarthur's fire-danger meters expressed as equations. *Austral Ecology*, **5 (2)**, 201–203.

Ohba, R., T. Hara, S. Nakamura, Y. Ohya, and T. Uchida, 2002: Gas diffusion over an isolated hill under neutral, stable and unstable conditions. *Atmospheric Environment*, **36 (36-37)**, 5697–5707.

Ray, P. S., 1986: Mesoscale meteorology and forecasting. *American Meteorological Society*, **1 (Chapter 20)**, 793.

Rothermel, R. C., 1972: A mathematical model for predicting fire spread in wildland fuels. *USDA Forest Service, Intermountain Forest and Range Experiment Station, Research paper INT 115. (Ogden, UT)*, 1–46.

Sun, R., S. Krueger, M. Jenkins, M. Zulauf, J. Charney, and F. USDA, 2009: The importance of fire-atmosphere coupling and boundary-layer turbulence to wildfire spread. *International Journalof Wildland Fire*, **18**, 50–60.

Taylor, P. A. and H. W. Teunissen, 1985: The askervein hill project: Report on the sept./oct. 1983, main field experiment. *Atmospheric Environment Service, Downsview, Ontario*, 1–314.

Undheim, O., H. I. Andersson, and E. Berge, 2006: Nonlinear, microscale modelling of the flow over askervein hill. *Boundary-Layer Meteorol*, **120 (3)**, 477–495.

Wang, W., C. Bruyère, M. Duda, J. Dudhia, D. Gill, H.-C. Lin, J. Michalakes, S. Rizvi, and X. Zhang, 2009: *ARW Version 3 Modeling System User's Guide*.

Zulauf, M., 2001: Modeling the effects of boundary layer circulations generated by cumulus convection and leads on large–scale surface fluxes. *PhD thesis, Univeristy of Utah*, 1–192.

Multi-scale Modeling of Wildfires 60NANB7D6144

Appended: The importance of Low-Level Environmental Vertical Wind Shear to Wildfire Propagation

by

Adam Kochanski, Mary Ann Jenkins, Ruiyu Sun,
Steven Krueger, Sepideh Abedi, and Joseph Charney

Accepted Oct 27, 2011, pending minor revisions by the International J. of Wildland Fire.

The Importance of Low-Level Environmental Vertical Wind Shear to Wildfire Propagation

Adam Kochanski[1], Mary Ann Jenkins[2], Ruiyu Sun[3], Steven Krueger[1], Sepideh Abedi[2], & Joseph Charney[4],

[1]Department of Meteorology, University of Utah, Salt Lake City, UT USA

[2]Department of Earth & Space Science & Engineering, York University, Toronto, ON, Canada

[3]Environmental Modeling Center, National Center for Environmental Prediction, Camp Springs, MD USA

[4]United States Forest Service, North Central Research Station, East Lansing, MI USA

Corresponding author:
Mary Ann Jenkins,
Department of Earth and Space Science and Engineering, York University,
Toronto, ON, Canada, M3J 1P3;
maj@yorku.ca; (416) 736 2100 x 22992.

Abstract

This study investigates the sensitivity of grassfire propagation to vertical shear in the near-surface environmental flow through four comparative grassfire numerical simulations with a coupled wildfire-atmosphere model. The model environment is prescribed by a uni–directional constant wind field, under neutral atmospheric conditions, with small surface friction, no Coriolis force or topography, and homogeneous fuel. By using the same near-surface (i.e., up to approximately 4 m above ground level) wind speed for all simulations, analyses of the output data can indicate if the behavior and spread rate of the fire depends on the interaction of the fire plume with the shear in the above-surface wind or on the magnitude of the mean upstream near-surface wind speed at the surface. Three aspects of wildfire behavior are investigated: the impact of uni-directional vertical shear on near-surface flow properties and fireline propagation; the variability in fire spread and area burnt due to the evolution of the surface flow; and the implications of low-level vertical wind shear on the prediction of wildfire, especially extreme or erratic, behavior.

1 Introduction

One wildland fire behavior that requires deeper understanding in order to further aid fire control and fire fighter safety is the propagation of the fireline. The question here is, can the propagation of a wildfire be forecast accurately based on solely the strength and direction of the mean upstream near-surface wind. In this present investigation we show that the answer to this question is no. Numerical model prediction of wildfire behavior and propagation cannot be "accurate" unless the coupling between the entire fire, including its plume, and the atmosphere is accounted for. Furthermore the existence of atmosphere/wildfire coupling means that prediction of wildfire behavior is never deterministic; it, like the evolution of atmospheric flow, is naturally subject to uncertainty. And finally, fire behavior can be very much affected by above-surface environmental wind conditions.

In this study, a coupled fire/atmosphere LES (Large-Eddy Simulator) is used to investigate the impact of a single environmental variable, the vertical shear in a uni-directional ambient wind field, on fireline propagation. By selectively varying the ambient vertical wind profile, we examine, through comparative numerical simulations under idealized atmospheric forcing, the influence of four different background vertical wind profiles — all with an identical upstream near-surface (i.e., at 1.5 m above ground level or AGL) wind speed — on the evolution of the spread of the surface fire perimeter.

In the forestry community, the traditional view is that a wildfire's spread rate depends on type and chemical composition of the fuels involved and the amount of energy released by their combustion, along with weather-related variables such wind strength and direction, and relative humidity, and topography and the behavior of the fire plume. The fire plume, also called the convection column, is tied to the combustion at the surface. The persisting paradigm for fireline propagation is that an ambient wind tilts the fire's convection column downstream and, therefore, the surface fire's flames as well. The greater the upstream near-surface ambient wind speed, the greater the tilt, and a tilted, as opposed to a vertical, flame heats and ignites the vegetation ahead more effectively through radiational heating and contact with ignition-temperature gases. Inherent in this prevailing paradigm is the view that only the impact of the near-surface wind on flame angle is relevant to fire spread.

The many operational wildland fire-spread models [e.g., Byram (1959); McArthur (1966, 1967);

Fosberg and Deeming (1971); Rothermel (1972); Van Wagner (1973); Albini (1976); Forestry Canada Fire Danger Group (1992); Balbi et al. (2007)], used by wildfire managers and fire fighters today, are based on the long-held concept of the role of near-surface winds on fire-flame geometry and fireline propagation. In these rate-of-spread formulations, the propagation of a fire front is generally modeled by a best-fit of experimental data or field observations to an exponential expression where fire spread depends either directly or geometrically on a near-surface flow. The definition of "near-surface flow" is not precise and depends on the particular fire-spread rate formula; in the Rothermel fire-spread model (Rothermel, 1972) for example, the near-surface flow is the wind speed at "mid-flame" height which operationally is measured as eye-level. For fire managers in the field, the near-surface flow is frequently the upstream mean near-surface wind (commonly from as far away as the nearest weather observing station) adjusted to calculate midflame-height speed.

It is the local flow in and around the fire, not an upstream mean surface wind, that propagates the fire's combustion, and this local flow is the result of fire-plume/atmosphere interactions. It is known by wildfire field operators and shown by researchers (e.g., Sun et al., 2009) that wildfire behavior can be influenced strongly by the evolution of the ambient flow in the atmospheric boundary layer through the feedback or coupling between the fire's combustion and convection column with the background flow. The atmospheric boundary layer, also referred to as the planetary boundary layer, can be as shallow as 500 m AGL or as deep as 3000 m AGL(Stull, 1988).

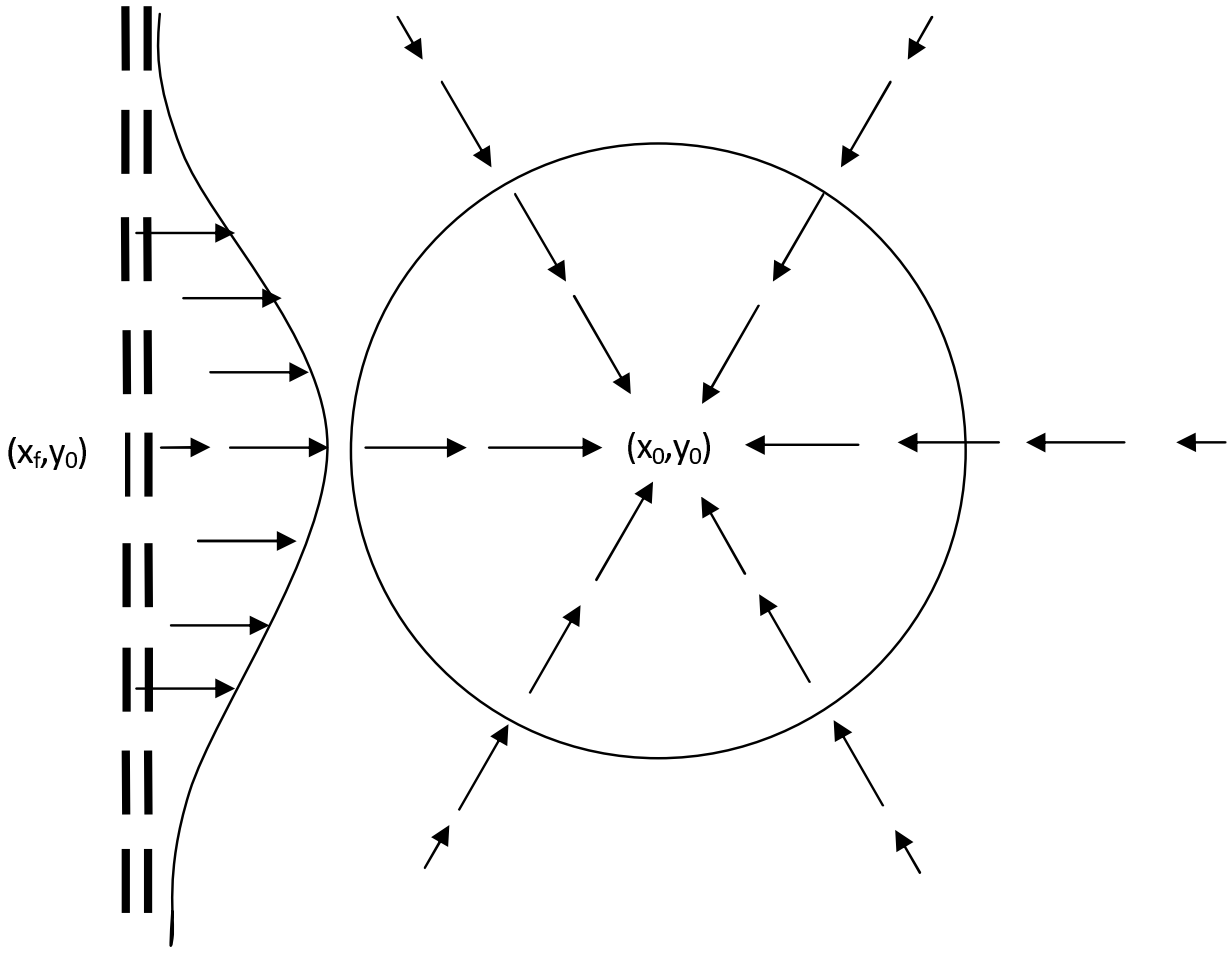

Figure 1: Idealized structure according to Clark et al. (1996a) of the near-surface convergence pattern in the vicinity of fire. See text for explanation.

Firelines tend to take on a "parabolic" shape when burning in an environmental wind field that is steady, constant with height, and directed perpendicular to the fireline (Cheney et al., 1993). Clark et al. (1996a) and Clark et al. (1996b) were two of the earliest efforts to employ a numerical prognostic cloud-resolving model coupled with an operational fire behavior model to study in a systematic way the sensitivity of fireline stability, geometry, and spread rate to an ambient wind field of this type. Figure 1 is a schematic of the idealized structure of the near-surface convergence pattern in the vicinity of a fire as described by Clark et al. (1996a). Clark et al. (1996a) explained the parabolic shape by considering the projection of the convergence in the near-surface flow produced by the convection column of the fire. When no ambient wind is present, a vertically-oriented convection column draws low–level air equally from all sides. When an ambient wind is present, the horizontal structure of the east-west component of the near-surface flow displaced horizontally

from the convection column has a bell- or parabolic- like shape with a maximum amplitude centered in the north-south direction of the cell. Clark et al. (1996a)'s explanation for the parabolic fireline shape could be called the "kinematic" explanation.

According to Clark et al. (1996a), the effect of downstream tilting of the convection column by a background wind is to shift the center of the low–level convergence pattern downstream, ahead of the fire front; the faster the ambient wind, the stronger the tilt, and the farther downstream the center of the convergence zone is positioned. However, because the magnitude of the constant background wind — and that of the near-surface wind — differed between experiments, it was not possible for Clark et al. (1996a) and Clark et al. (1996b) to decide if or how much the downstream projection of the convergence zone depended on the strength of the upstream mean near-surface wind as opposed to near-surface wind features that were the result of interactions of the convection column with the above-surface wind conditions. This is the question therefore that we wish to examine here.

This study is organized as follows. In Section 2 the experimental setup and initialization of the flow for four coupled fire/atmosphere Large-Eddy Simulations are described. In each, the upstream near-surface wind is identical, while the above-surface mean wind profile is not. In Section 3, the equations used to investigate the differences in the near-surface local flow in and around the fire are introduced. Output from four LES-fire simulations is used to calculate the relevant fields introduced in Section 3, and these fields are presented and discussed in Section 4. In Section 5, results of the study are summarized, the major conclusions are discussed, and suggestions for future work are made.

2 Numerical Experimental Set-up

To achieve our objectives, we used the LES version of the WRF (Weather Research and Forecasting) model (Wang et al., 2009) coupled with SFIRE, the wildland surface fire module (Mandel et al., 2008, 2011), to simulate moving grassfires.

In the WRF-SFIRE model domain a (x,y,z) grid mesh of (320,160,81) nodes was used where the horizontal grids intervals were $(\Delta x,\Delta y)$= 20 m, making the (x,y,z) domain dimensions (6400 m, 3200 m, 3900 m). For the WRF-SFIRE's surface fire grid (Mandel et al., 2008, 2011), the

fire-to-atmosphere refinement ratio was set to 10, which translates into fire domain grid intervals of $(\Delta x,\Delta y)_f$= 2 m. A hyperbolically-stretched vertical grid was used, with a minimum vertical Δz grid size of 1.5 m in the first grid level. The model time step was 0.02 s. Open boundary conditions (Klemp and Lilly, 1978) are applied on the lateral and top boundaries. All simulations are 1800 s (30 minutes) long and output files were saved every 5 seconds. The sizes of time step, grid lengths, model domain, and simulation time, along with frequency of output, were dictated by computer resources and numerical stability. Each simulation was performed on 136 cores (34 Quad Xeon processors at 2.8 GHz = 17 dual Quad Xeon Nodes with Infiniband interconnects at 8 cores each) and simulation wall-clock times ranged between approximately 15.25 to 17.5 hours. Each simulation used roughly 3.5GB of RAM, and the output files from each simulation required approximately 250GB of storage.

Initial fireline length and width were 400 and 20 m, respectively, and initial fuel load was 0.626 kg m^{-2}. Roughness height was 0.036 m, which remained constant before and after the grass was burnt; WRF-SFIRE has currently no option to diminish surface roughness in burnt-out areas. The background temperature profile was a uniform potential temperature of 300K. With the exception of one simulation, each initial fireline was located 2000 m in the positive x (east-west) direction. In the TANH fire, the initial fireline was located 4000 m in the positive x direction. All firelines were centered in the y (north-south) direction.

Four WRF-SFIRE numerical experiments are presented. The four simulations, called CONTROL, LOG, SHEAR, and TANH, are of propagating grass fires, burning in uniform fuel on level terrain, each initialized as a straight line perpendicular to the direction of a westerly background wind. Figure 2 shows the westerly background wind as a function of height that was applied at the model's inflow boundary for each experiment. All experiments have the same upstream initial environmental surface (i.e., at the first grid level) wind speed but different above-surface wind profiles. In each case, the environmental near-surface wind speed is directed from west to east, in the positive x direction of the model domain, and equal to 5.5 m s^{-1}.

By selectively varying the ambient vertical wind profile, it is possible through comparative numerical simulations with the WRF-SFIRE model to examine, under idealized atmospheric stability and wind conditions, the influence of different background vertical wind shears on the evolution of the fire plume and near-surface spread of the fire perimeter. CONTROL is the simulation in

which a constant background wind (red plus signs in Figure 2) was applied at the model's inflow boundary. CONTROL illustrates the evolution of a grassfire burning in an environment of constant westerly flow with no above-surface vertical wind shear and serves as the prototype for comparison with the other simulations. In LOG, the vertical distribution of the westerly background inflow (green asterisks in Figure 2) is prescribed by the log-linear wind profile based on a near-surface wind of 5.5 m s^{-1} and a roughness height of 0.036 m. A slightly negative linear-sheared background wind profile (where the wind blows faster at the surface than aloft) is used in SHEAR (blue squares in Figure 2). In TANH the low-level shear in the background wind profile is strongly negative. The tanh background wind profile (dark purple triangles in Figure 2) varies from 5 m s^{-1} near the ground, changes sign at $z = 250$ m, and is asymptotic to -5 m s^{-1} aloft. As noted by Clark et al. (1996b), this type of ambient wind-shear occurs in gust fronts, convective downdrafts, and mountain valley flows. Each fire's plume also experiences difference upper-level wind strengths; the magnitude of the upper-level zonal flow is strongest in the LOG fire ($\sim$ 15 m s^{-1}), weakest in the SHEAR fire ($\sim$ 3 m s^{-1}), and moderate ($\sim$ 5.5 m s^{-1}) in the CONTROL and TANH fires.

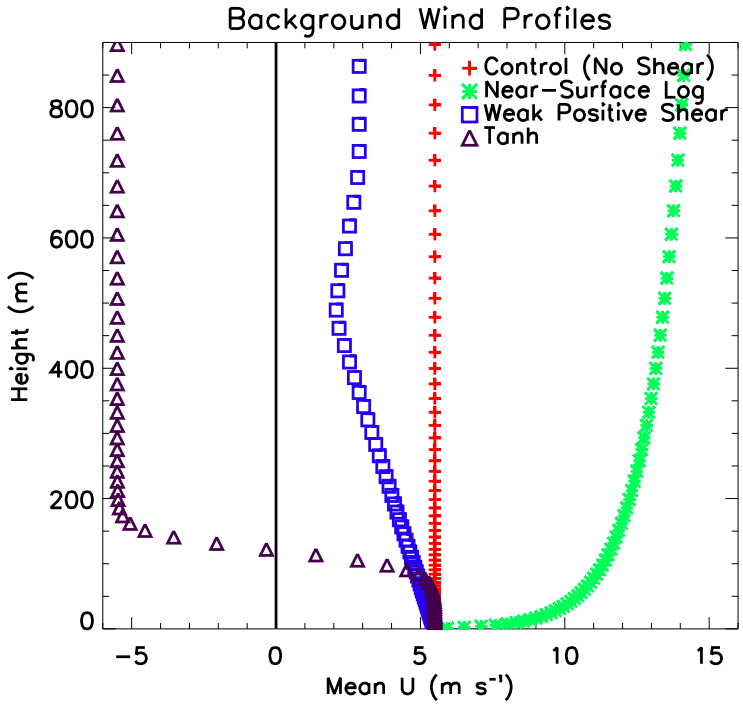

Figure 2: Vertical profiles of the $\overline{u}(z)$, background wind, used in coupled WRF–SFIRE experiments CONTROL (red plus signs), LOG (green asterisks), SHEAR (blue squares), and TANH (dark purple triangles). See text for further explanation.

3 Flow Features

A few basic features associated with the evolution of the surface flow are used to illustrate the impacts that the different upstream above-surface background wind fields (Figure 2) have on the spread of a fireline. In the following, subscripts (x,y) denote differentiation with respect to (x,y) and superscripts denote (x,y,z) components.

Near-surface flow due to fire/atmosphere interactions is described by the magnitude of the perturbed horizontal wind vector, which expressed mathematically is

$$|\vec{V}_H'| = \sqrt{(u - \overline{u})^2 + v^2}, \tag{1}$$

where $\vec{V}_H$=($u\,\widehat{i}, v\,\widehat{j}$), is the horizontal (denoted by subscript H) wind vector, (u,v) are (x,y) components of the flow, and ($\widehat{i}$, $\widehat{j}$) are (x,y) unit vectors in the Cartesian coordinate system. The overbar ($\overline{\ }$) denotes the base state or mean state, and $\overline{u}(z)$ represents the background wind profile that is a function of height z only. The prime ($'$) denotes the deviation or fluctuation from the base state. Here $u = \overline{u}(z) + u'$ and $v = v'$. It is $\overline{u}(z)$ for each numerical experiment that is displayed in Figure 2.

Separation and coming together of flow parcels in the x-y plane are described by horizontal divergence, δ, which expressed mathematically is

$$\delta = \nabla_H \cdot \vec{V} = u_x' + v_y', \tag{2}$$

where $\delta > 0$ signifies divergence and $\delta < 0$ signifies convergence of flow parcels.

The spin or rotation of flow parcels in the x-y plane is described by ζ^z, the component of the vorticity (i.e., fluid rotation at a point) vector in the vertical (z) direction, which expressed mathematically is

$$\zeta^z = v_x' - u_y', \tag{3}$$

where $\zeta^z > 0$ signifies cyclonic or counter-clockwise rotation and $\zeta^z < 0$ signifies anticyclonic or clockwise rotation of flow parcels in the x-y plane.

One reason vorticity is often a distinctive feature in atmospheric flows is its attribute of per-

sistence. When a region of fluid acquires vorticity, this flow pattern tends to last a relatively long time compared to other flow patterns on the same scale. Vortices arise within a flow containing vorticity and tend to be associated with discrete, nearly circular extrema of vorticity. In a wildfire it is not unusual for the magnitude of vertical vorticity in a vortex to reach that for supercell-storm tornadoes, which is approximately 0.3 to 1.2 s^{-1} (Bluestein et al., 1993). In the following Section, where the results of the numerical experiments are presented, it will be seen that vertical vorticity and vortices are common and lasting features of the fire dynamics.

4 Experimental Results

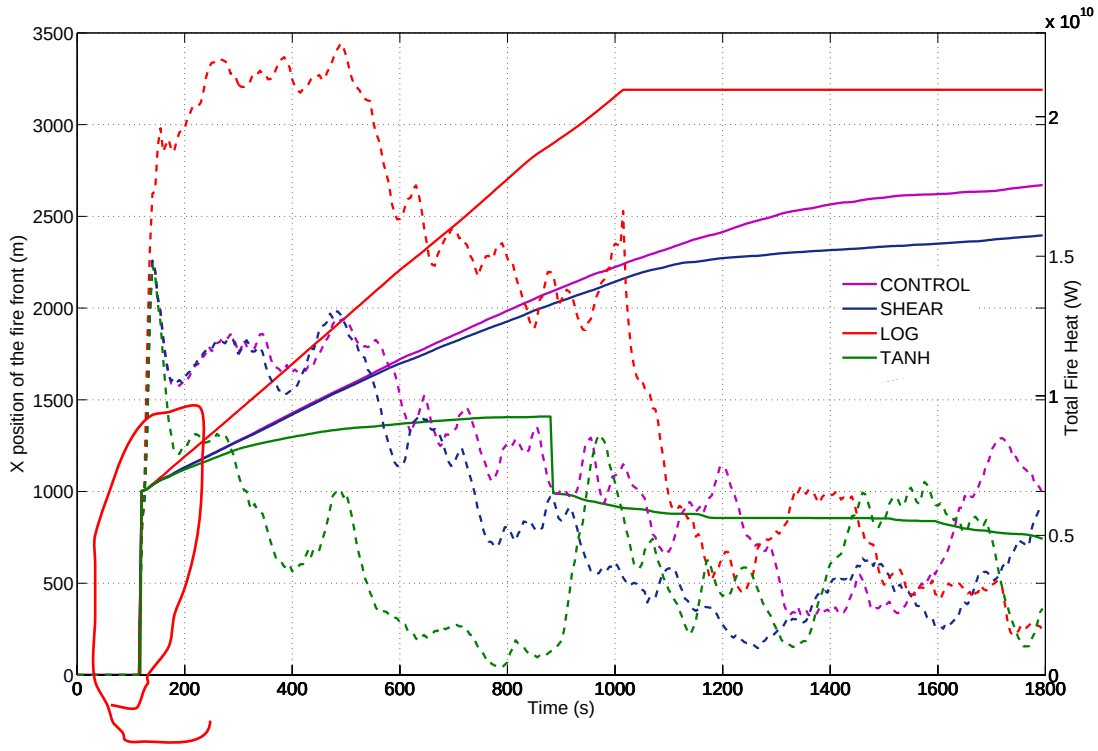

Figure 3: Time series of the fire front positions in the x direction (solid lines), and the instantaneous total heat-release rates in the fire domain (dashed lines), for CONTROL (purple), SHEAR (navy), LOG (red) and TANH (green) fires.

The fire-front positions and total heat-release rates as functions of time for each simulation are shown Figure 3. The position of the fire front was determined from the average forward movement

of the fire front; an examination of the rate-of-spread data at 5-second intervals The CONTROL, LOG, SHEAR, and TANH fires with, respectively, ambient constant, near-surface log, and weakly negative, and hyperbolic-tan vertical shear uni-directional wind profiles, show that fire-domain total heat-release rates peak with ignition, quickly equilibriate, steadily decline during the first 800 to 1000 seconds, and then level off after that. The larger the fire-spread rate the more intense the fire. Before $\sim$ 1000 seconds, depending on the vertical structure of the background wind, the fire front moves either extremely slowly (e.g., the TANH fire), or slowly (e.g., the SHEAR fire) or very quickly (e.g., the LOG fire), or somewhere in between (e.g., the CONTROL fire), even though the upstream mean near-surface wind of all fires is the same. At 300 s (5 minutes) into the simulations, the plume, updraft, and front of each fire are well developed. After 600 s, the strengths of the fire-induced winds and plume updrafts in the CONTROL, SHEAR, and LOG fires decrease gradually with time, as each fire's head, perimeter, and active burning area narrow and stretch, causing the total fire domain heat-release rate to decline.

From the very beginning, the TANH fire propagated more slowly than the other fires and evolved in a completely different way. The heat-release rates in the TANH fire decrease with time to almost nil at 900 seconds, and then increase again to match the heat-release rates of the other fires. This heat-release rate behavior is consistent with the relatively slow forward (eastward) propagation of the TANH fire front during the first 900 seconds. Figure 3 indicates, however, that 900 seconds into the simulation is a critical moment in the TANH fire; the foreward movement of the fire front stalls and fire-induced surface winds become suddenly extremely erratic. After this point, the TANH fire develops an active fire front in a different section of the fire's perimeter that moves westward, not eastward. Near the end of the simulation the most active section of the TANH fire perimeter was the south-west section, where the surface wind pattern was affected by the formation and then movement of strong vertical vortices around and into the fireline.

For the first 1000 seconds, the LOG fire had the fastest forward propagation speed and consequently the greatest heat-release rate. The fire spread rates plotted in An examination of the rate-of-spread data at 5-second intervals shows that rate-of-spread at the head of the LOG fire almost always reached the limiting value (approximately 6 m s^{-1}) allowed by the rate-of-spread formulation used in WRF-SFIRE (Mandel et al., 2008, 2011). After 1000 seconds, the LOG fire front was out of the fire domain, which explains why Figure 3 shows a constant fire front position

from then on. The LOG fire's declining total fire-domain heat-release rates in Figure 3 after 1000 seconds are from only the portion of the LOG fire perimeter still within the fire domain.

In order to understand the evident differences between the fires seen in Figure 3, an examination of the surface flow features calculated using Equations 1, 2, and 3 are presented next, where the terms "surface" or "near-surface" are defined as 4 m AGL (height of second vertical grid level). The analyses illustrate some important differences between the coupled fire/atmospheric flows for each fire and the impacts they have on fireline propagation. Relevant results from simulation times 300, 600, 900, 1200, 1500, and 1795 seconds are chosen for discussion. The analyses of the SHEAR fire are described but not shown.

4.1 Results at 5 Minutes – Initial Steady-state for all Fires

Figures 4 to 6 display the horizontal cross sections of the properties determined by Equations 1, 2, and 3 at 300 seconds (5 minutes) and at 4 m AGL (above ground level).

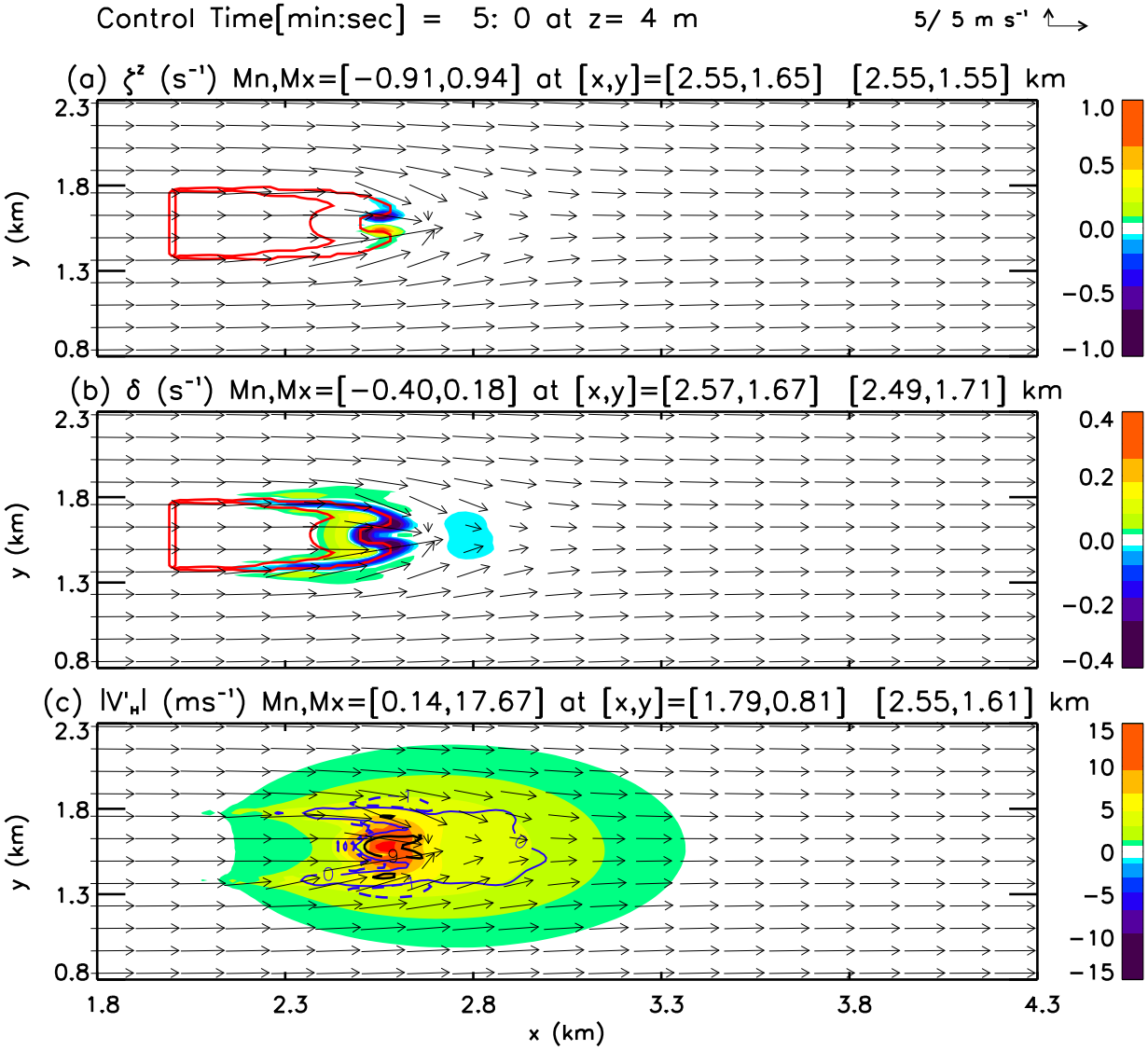

Figure 4: Horizontal cross sections for z= 4 m of (a) vertical z vorticity ζ^z (s^{-1}), (b) horizontal divergence δ (s^{-1}), and (c) wind speed perturbations $|\vec{V}'_H|$ (m s^{-1}) at 300 seconds for the CONTROL fire. Magnitudes of each contour are indicated by colors in bar plots on the right. For each field, minimum and maximum values, plus their (x,y) positions on cross section are given. Vectors denote background plus perturbed wind components in x-y plane where magnitude is scaled as indicated in top right corner of plot. Red contours in (a) and (b) outline the fire (i.e., burning surface area) perimeter. Contour lines in (c) delineate negative (dashed blue), zero (solid blue), and positive (solid black) vertical velocity component w values at approximately 100 m AGL. Note that the (aspect) ratio between the width of the image to its height is not equal to one; consequently all plots show features lengthened in the horizontal direction compared to the vertical direction.

The front of the CONTROL fire has moved a little more than half a kilometer forward (0.55 km in the positive x direction) since ignition. There is strong convergence along the forward fire

perimeter and fire head (Figure 4b) as the fire-induced flow comes together at the base of the fire's convection column (Figure 4c). The solid black lines in Figure 4c show the 9 m s^{-1} contour for w, the vertical wind component at 100 m AGL. The maximum w at this AGL was 18 m s^{-1} at (x,y) = (2.57, 1.63) km, co-located with the maximum convergence in the near-surface flow below. The minimum w was -4 m s^{-1}, at (x,y) = (2.57, 1.33) km, and along the fire's flank. The westerly mean flow is normal to the ignition line, and the fields in Figure 4 are symmetrical with respect to the central east-west axis of the fire. The areal extent of the surface flow influenced by the CONTROL fire's convection is approximately half a kilometer ahead, behind, and on either side of the front front (Figure 4c).

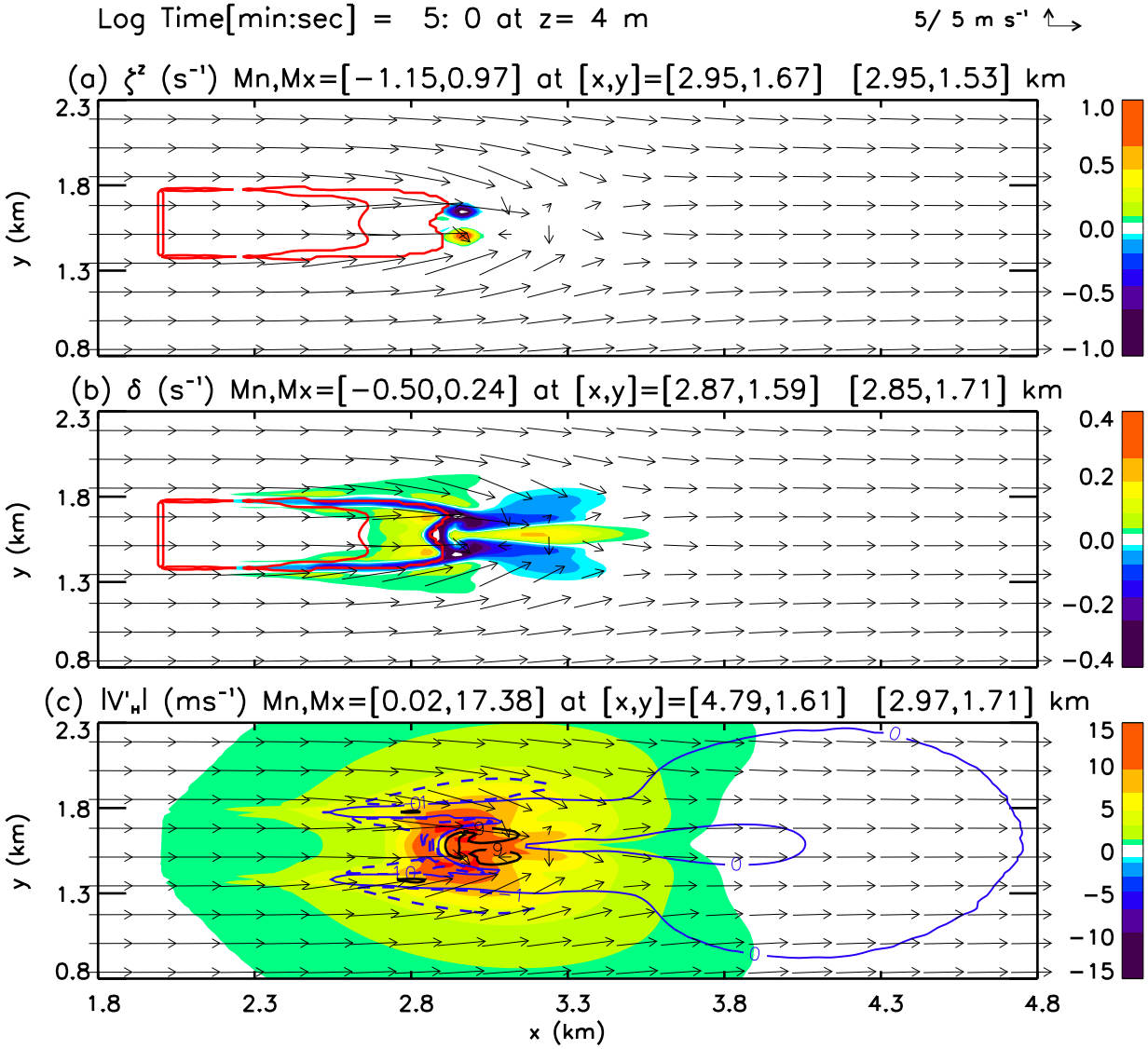

Figure 5: As in Figure 4 except for 300 s into the LOG simulation.

The CONTROL fire (Figure 4) shows the surface convergence pattern and winds in the vicinity of the fire front pulling the fire front into an inverted near-parabolic shape. An inverted parabolic shape is not the idealized shape of the fire front displayed in Figure 1. Furthermore, three-dimensional animation and examination of the data show that there is a vortex couplet associated with the CONTROL fire front: the vortex couplet is two distinct, coherent, equal-magnitude, persistent counter-rotating vertical vortices located at the fire's head that, in the CONTROL fire, are embedded in the fire front (Figure 4a).

The vortex couplet is an important feature of the fire head; the results suggest that the vortex

couplet provides the inverted parabolic shape to the fire front, enhances the local surface wind speed, and is closely co-located with the convergence and wind speed perturbation maxima in the flow. The x locations (2.55 km) of the two vortices (Figure 4a) match the x position of the maximum fire-induced surface wind speed (Figure 4c), which is almost 18 m s^{-1} and occurs a little behind the convergence maximum at x=2.57 km (Figure 4b). Despite the inverted parabolic shape of the fire front, the positioning of these features are consistent with the idealized surface flow depicted in Figure 1.

Figure 4a shows that the cyclonic and anticyclonic rotations of the southern and northern vortices, respectively, of the couplet are almost equal in magnitude and strength (i.e., $\sim$ 1 s^{-1} which is tornado-strength). In a uniform flow, two vortices having opposite rotation of equal strength do not rotate around each other, but move along with this flow in straight lines parallel to each other (Markowski and Richardson, 2010). The CONTROL vortex couplet is expected, therefore, to behave in this fashion unless the wind field that the vortex couplet is embedded in becomes non-uniform (i.e., is perturbed) and/or the rotation rates of the vortices become unequal.

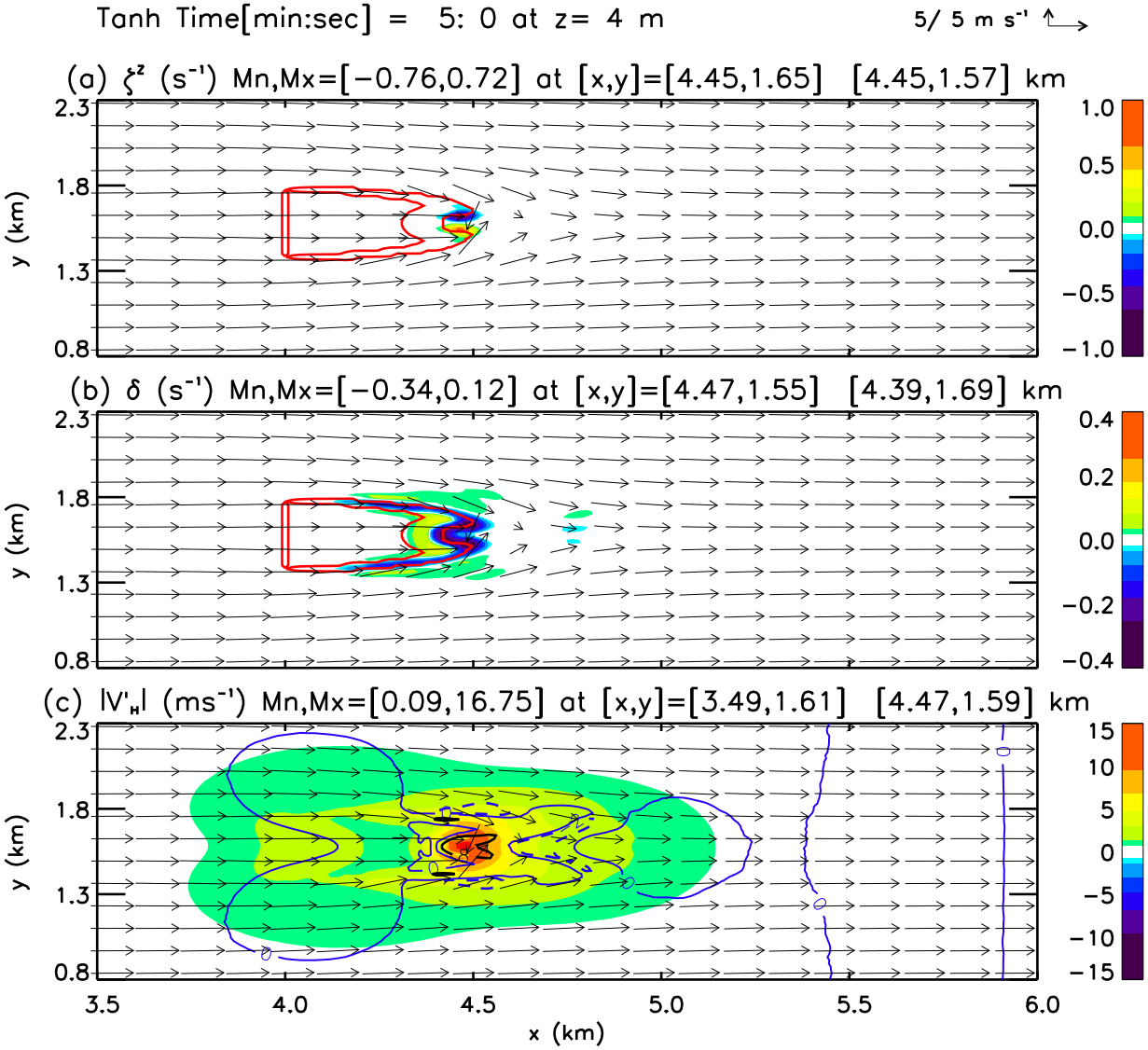

Figure 6: As in Figures 4 to 5 except for 300 s into the TANH fire simulation.

There are only slight differences in the flow properties and locations of maxima and minima between the CONTROL fire (Figure 4) and the SHEAR fire (not shown). As in the CONTROL, the SHEAR fire forms a vortex couplet that shapes the fire front, enhances the local surface wind speed, and is co-located with the convergence maxima in the flow. The slightly negative vertical shear in the background wind does not appear to impact the fire behavior in any significant way except that the magnitudes of flow properties and forward fireline propagation are slightly smaller in the SHEAR fire compared to the CONTROL.

The same cannot be said of the LOG fire (Figure 5). The obvious differences between the

surface flow features in the LOG fire compared to the CONTROL are: the much larger areal extent of surface flow influenced by the LOG fire (Figure 5c); a different placement and configuration of the vortex couplet and divergence-convergence pattern associated with the fire front (Figure 5a,b); a deeper fire front; and a greater forward movement of the fire front (approximately 0.85 km in the positive x direction over the last 5 minutes). At 300 seconds, for every fire, there is moderately strong divergence in the surface flow approaching the base of the convective updraft, followed by strong convergence in the surface flow just at the tip and ahead of the burning fire front. The highs and lows in this west-to-east pattern of divergence/convergence are weakest in the TANH fire (Figure 6b) and strongest in the LOG fire (Figure 5b). Figure 5b shows how, even further forward, the LOG fire has a north-south convergence/divergence/convergence surface pattern. The LOG fire shows strong surface divergence in the center of the domain accompanied on each side by two symmetrical convergence zones that extend almost 0.5 km ahead of the fire front. Figure 5c shows how much further forward the w at 100 m AGL extends. The areal extent of the surface flow influenced by the LOG fire is nearly a kilometer ahead and behind the front front (Figure 5c).

It is likely that the differences in the surface divergence pattern in the LOG fire compared to any of the other fires are due to the position and strength of the LOG vortex couplet. Compared to the CONTROL fire, the x position of the LOG vortex couplet is out ahead of, not embedded in, the fire front. The x position of the LOG vortex couplet (2.95 km; Figure 5a) matches closely the maximum $|\vec{V}_H'|$ (17.4 m s^{-1} at x= 2.97 km; Figure 5c). Unlike the CONTROL fire, the vortex couplet and $|\vec{V}_H'|$ maximum in the LOG fire lead the convergence maxima (x= 2.87 km; Figure 5b) by about 100 m. The stronger fire-induced surface winds associated with the vortex couplet are consistent with greater convergence in the surface flow just ahead of the fire front and greater divergence in the surface flow out ahead of that, and are part of the near-surface wind pattern associated with the more near-parabolic shape of the LOG fire front; the tip of the LOG fire front has a less concave shape than that of the CONTROL fire front. The distance separating the rotating columns of the vortex couplet is also larger in the LOG fire compared to the CONTROL. Furthermore, the maximum w at 100 m AGL was 19 m s^{-1} at (x,y) = (3.05, 1.53) km, co-located, not with the convergence maximum in the surface flow, but with the x position of the vortex couplet.

Figure 6 shows that, even though the general patterns of vorticity, divergence and wind speed perturbations in the TANH fire resemble the ones from CONTROL fire, there are also obvious

differences between them. Magnitudes of flow properties, the areal extent of the surface flow influenced by the fire's convection column, depth of the fire front, and forward fireline propagation are noticably smaller in the TANH fire compared to the CONTROL. While the CONTROL and LOG fires have propagated by as much as 0.55 and 0.85 km forward, respectively, the TANH fire front has moved only approximately 0.45 km forward. Furthermore, Figure 6c indicates perturbed flow behind (i.e., to the west of) the TANH fire, while in the CONTROL, SHEAR (not shown), and LOG fires, flows were perturbed only ahead of the fires. In the TANH fire, the strongest w at 100 m AGL, and surface convergence, vorticity, and $|\vec{V}_H'|$ are all located over and along the leading edge of the fire front. In Figure 6c, the maximum w at 100 AGL was 16 m s^{-1} at (x,y) = (4.49, 1.57) km, located above the maximum convergence in the surface flow.

The background wind field in the CONTROL fire has (except for a very shallow surface shear due to surface roughness) no shear, the SHEAR fire has slightly negative linear vertical shear, the LOG fire has large surface positive vertical shear, and the TANH fire has intense negative vertical shear. Note, however, that the directions of rotation in the vortex couplets associated with the fire fronts are the same for all four fires. This suggests that the vertical shear in the background wind is not responsible for the direction of rotation in the vortex couplet and that vorticity of significant magnitude seen in Figures 4a, 5a, and 6a is fire-induced.

Figures 7, 8 and 9 show the flows associated with plume development at 300 seconds into the CONTROL, LOG, and TANH simulations. The y and x intersect positions of the vertical cross sections in these figures are chosen to capture each fire plume's updraft core. The most obvious differences between the fire plumes are their tilts with height and the increased widths of the fire plumes with increased tilts. Depending on the vertical structure of the upper-level ambient wind, the tilts of the fire plumes are: almost upright in the CONTROL fire (Figure 7a), slightly upwind (i.e., westward) in the TANH fire (Figure 9a), and downwind by almost 45 degrees with respect to the surface in the LOG fire (Figure 8a).

Given that the fire spread and heat-release rates are greatest in the LOG fire, it might be assumed that its maximum updraft speed is also greatest. This does not appear to be the case. The maximum updraft speeds along the central x-z plane of each fire are: 30 m s^{-1} at $\approx$ 400 to 600 meters AGL in the CONTROL fire (Figure 7a); 20 to 25 m s^{-1} at $\approx$ 400 to 700 meters AGL in the LOG fire (Figure 8a); and 25 m s^{-1} at $\approx$ 500 meters AGL in the TANH fire (Figure 9a).

The maximum updraft speeds in the y-z plane along each fire front are: 15 m s^{-1} at $\approx$ 650 meters AGL in the CONTROL fire (Figure 7b); 20 m s^{-1} at $\approx$ 400 to 700 meters AGL in the LOG fire (Figure 8b); and 12 to 16 m s^{-1} at $\approx$ 200 to 400 meters AGL in the TANH fire (Figure 9b).

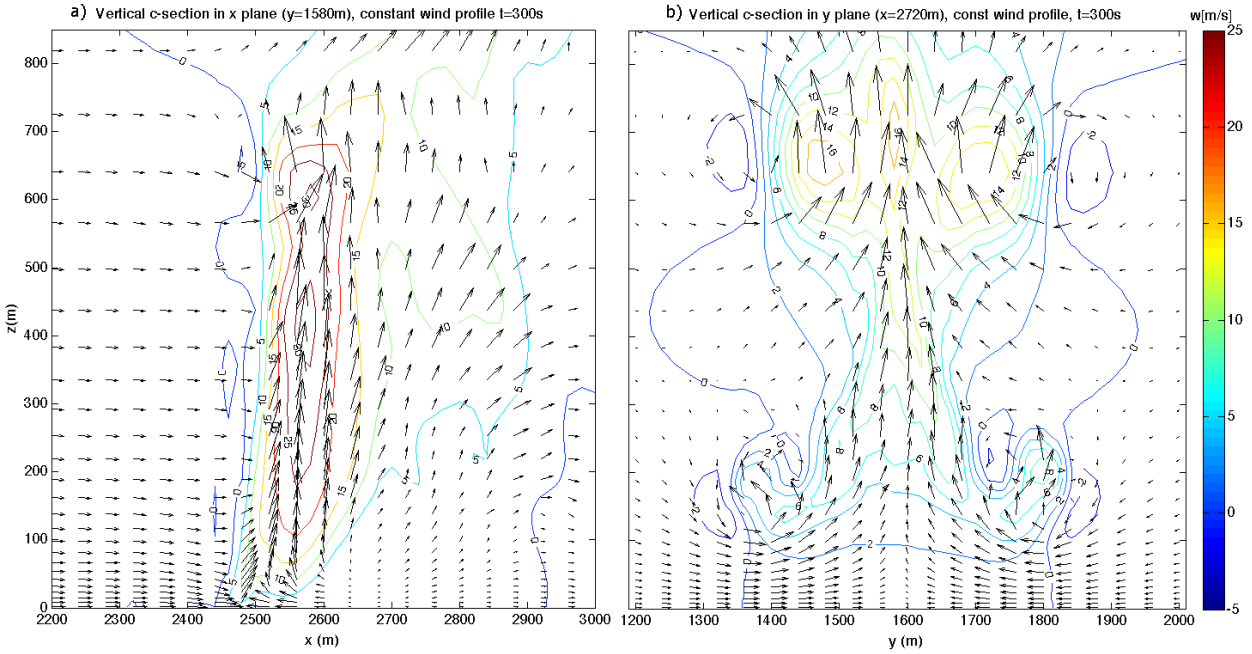

Figure 7: Vertical cross sections of the flow in the (a) x plane at y= 1580 m and the (b) y plane at x= 2720 m at 300 s into the CONTROL fire simulation. Contour lines represent the vertical velocity component w.

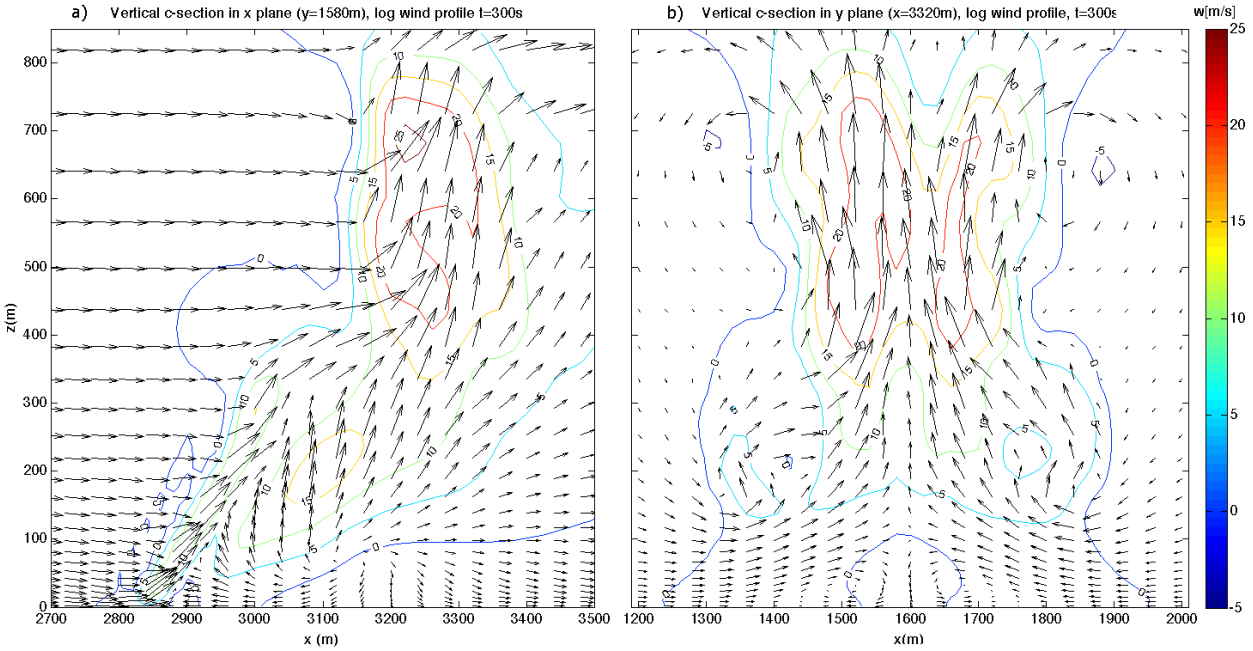

Figure 8: Vertical cross sections of the flow in the (a) x plane at y= 1580 m and the (b) y plane at x= 3320 m at 300 s into the LOG simulation. Contour lines represent the vertical velocity component w.

In general, the tilted the plume, the more adversely affected the plume updraft speed is by entrainment (Markowski and Richardson, 2010). A tilted plume enhances entrainment of ambient air, leading to plume expansion and a reduction in the temperature excess and therefore buoyancy in the plume core. And in general, fire plumes that are wider experience a greater downward-directed buoyancy pressure gradient force (Houze, 1993) that acts against an upward-directed buoyancy force. It is probably valid to assume that plume tilt is the reason why the LOG fire has the widest (based on the w fields displayed in Figure 8) plume, while the CONTROL fire has the strongest updraft. Differences in plume tilts may be at least partly responsible for the differences in location and magitude of maximum updraft speeds in the fire plumes.

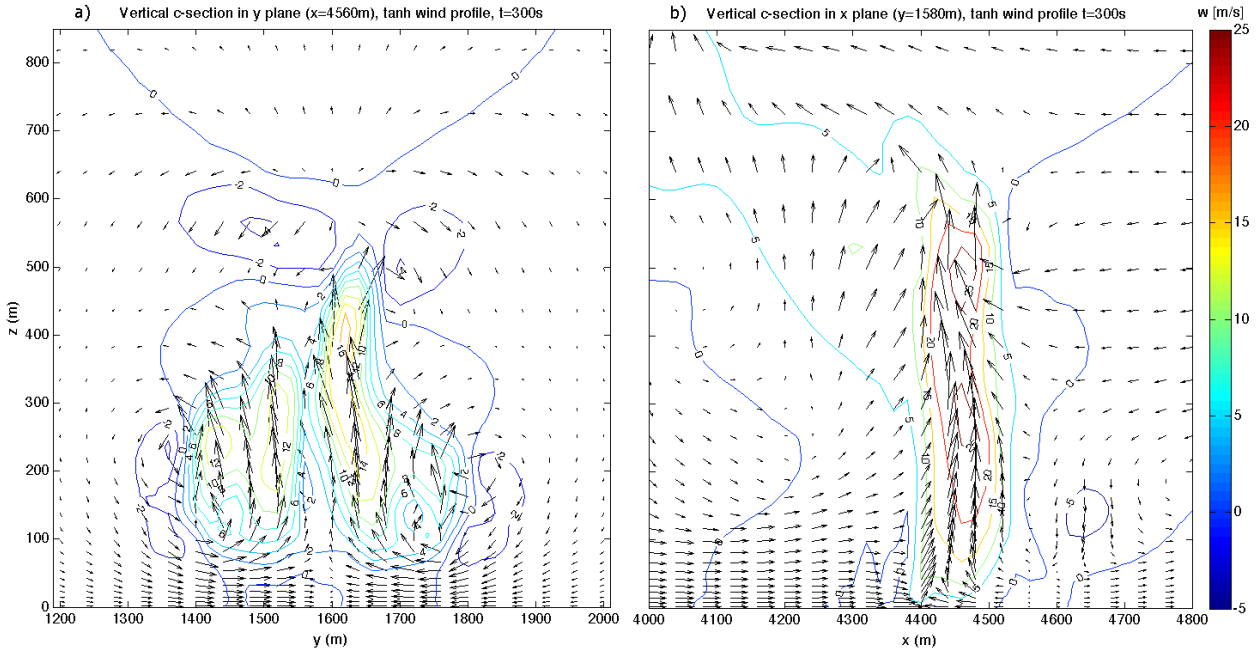

Figure 9: Vertical cross sections of the flow in the (a) y plane at x= 4560 m and the (b) x plane at y= 1580 m at 300 s into the TANH fire simulation. Contour lines represent the vertical velocity component w. **For reviewers: switch a,b in Figure 9. Text is written to reflect this.**

Since the strongest updraft occurs in the CONTROL fire, it might be expected that the strongest fire-induced surface convergence occurs in the CONTROL fire. However, this too is not necessarily the case; the strongest fire-induced surface convergence is observed in the LOG, not the CONTROL, fire. In the LOG fire, a concentrated, strong, narrow updraft did begin close to the surface (Figure 8a). The factors associated with the LOG fire's greatest forward rate-of-spread compared to the CONTROL, SHEAR or TANH fires appear to be connected with the strong surface convergence and rotation of the vortex couplet, and their locations out ahead of the fire front.

Figures 4 to 6 and Figures 7 to 9 all show flow separation upstream of the fire front. This surface flow feature is most distinct in the LOG fire, occurring approximately 380 m ahead (at approximately x= 3200 m in Figure 8a) of the fire front, at the bottom of a downdraft that originates approximately 100 m AGL. The downdraft penetrates to the surface and leaves its footprint in the form of relatively strong surface divergence upstream and strong convergence downstream (Figure 5b) in the flow between the counter-rotating columns of the vortex couplet (at y= 1580 m in Figures 8b and 8a). As discussed in connection with Figure 5, this flow feature, along with the vortex couplet, appears to strengthen surface convergence and wind into the base of the LOG fire

plume. Although there is a downdraft and surface flow separation ahead of the CONTROL and TANH fires, they are smaller in magnitude and areal extent compared to the LOG fire. It may be that in the TANH fire this circulation is associated with the reversal in the ambient flow rather than a fire-induced circulation; the downdraft maximum is observed around 150 m AGL, exactly where the TANH ambient wind changes direction from westerly to easterly. The elevation of the TANH downdraft maximum seems to be too high to allow for penetration of the downdraft below 50 m AGL, and consequently there is no divergence in the flow ahead of the TANH fire front (Figure 6b).

Figures 7b, 8b and 9b show that flow-property symmetry with respect to the central east-west axis of the fire is evident in the CONTROL and LOG fire plumes, less so in the TANH. An analyses of the model output indicates that this asymmetry in the TANH plume at 300 s grows greater over time. Figures 7, 8 and 9 also show how much taller the LOG and CONTROL plumes are compared to the TANH.

4.2 Results at 10 Minutes – Steady-State

The properties displayed in Figures 10, 11, and 12 are the same as those displayed in Figures 4, 5, and 6, except for 600 seconds (10 minutes) into the simulations.

A comparison of flow properties for the CONTROL fire at 600 s (Figure 10) to those at 300 s (Figure 4) shows that the fire front is maintaining its near-parabolic shape, having moved forward by approximately .90 km in the last 5 minutes, with a slight drop in the magnitudes of divergence and wind speed perturbation maxima and minima, while the areal extent of the surface flow influenced by the fire's convection column has grown (Figure 10c). The fields in Figure 10 are still symmetrical with respect to the central east-west axis of the fire.

The surface strength of the CONTROL vortex couplet is significantly less than it was at 300 s. Even though the general shape of the fire front is conserved, its head is smaller due to a decrease in the size of, and separation distance between, the rotating columns in the vortex couplet. In the CONTROL fire, as well as the SHEAR and LOG fires, the vertical vortices in the couplet have moved closer to each other; this change is attributed to non-uniformity in the fire-induced flow and the discrepancy in magnitude of rotation between the counter-rotating vortices in the vortex pair. To a great extent, however, the vortex couplet is behaving as expected; the vortices have continued

to move parallel to each other, in the same direction as the background (westerly) flow.

The reduction in size of the vortices, however, is evident only close to the surface. An examination of the data shows that the columns in the vortex couplet form a narrow V-shape in the vertical, spreading apart further with height; the V-shape configuration gives them more space at higher levels, allowing for their horizontal growth with height.

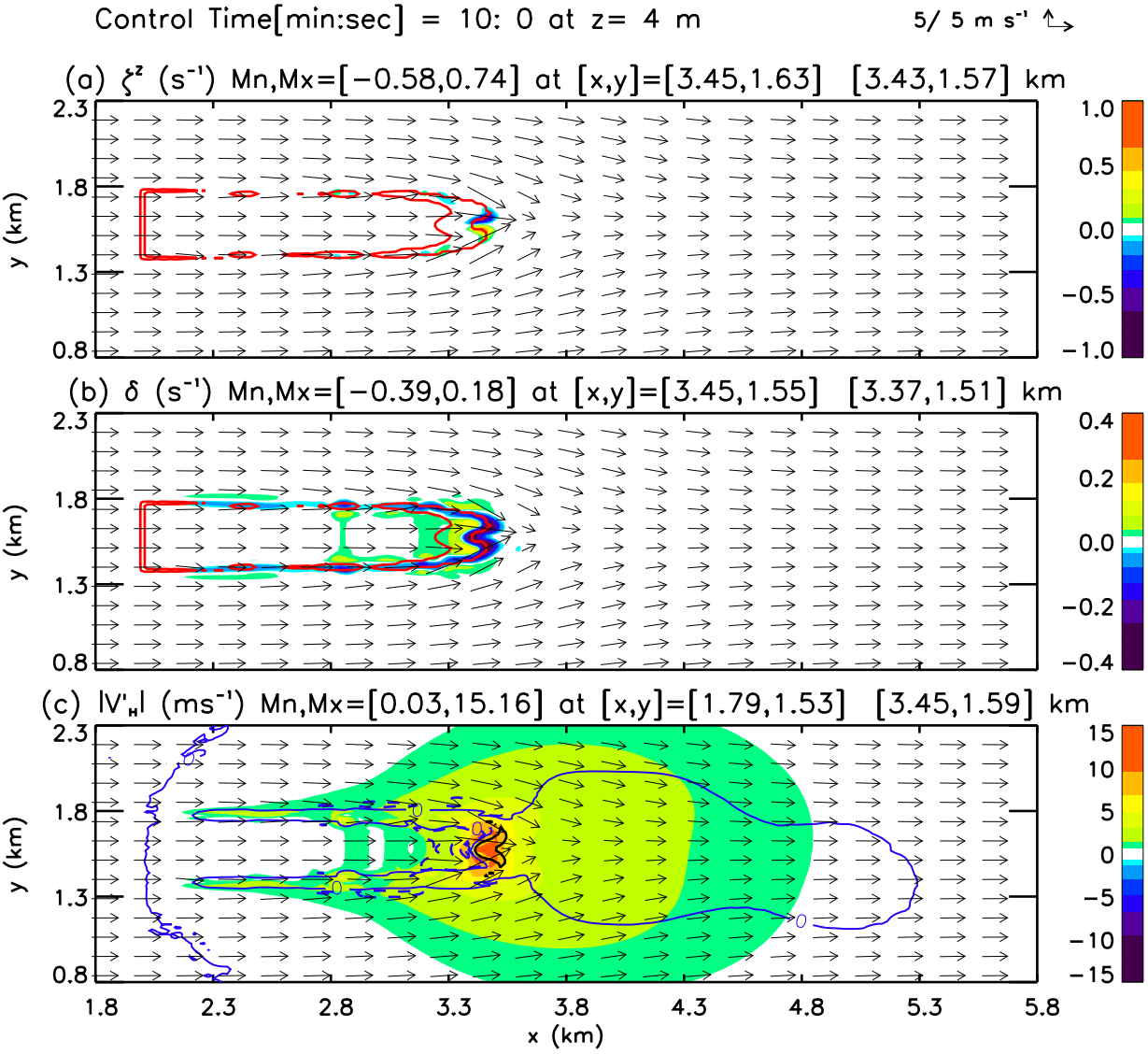

Figure 10: As in Figure 4 except for 600 seconds into the CONTROL fire simulation.

The CONTROL fire plume at 600 s (not shown) is very similar to the one observed at 300 s (Figure 7), but with slightly more downwind tilt and greater vertical extent. The maximum

magnitude in the fire-induced updraft (33 m s^{-1}) is practically the same as 5 minutes earlier. However, since the most active updraft is now located higher near $\sim$ 1500 m AGL, as opposed to $\sim$ 650 m AGL at 300 s, its influence on the flow is diminished. The associated surface convergence in the flow is weaker, the weak convergence in the surface flow out ahead of the fire front at 300 s (Figure 4b) is gone, and the maximum in the fire-induced surface wind perturbation has decreased (15.2 m s^{-1} at 600 s versus approximately 17.7 m s^{-1} at 300 s).

Again the magnitudes of flow properties and forward fireline propagation are slightly smaller in the SHEAR fire (not shown) compared to the CONTROL (Figure 10). The impact of weak negative vertical shear in the background wind on the SHEAR fire appears to be a consistently slightly slower forward fireline propagation.

Near-surface shear in the wind profile in the LOG fire does impact fire behavior and fireline propagation in significant ways. Figure 11 shows that the fire front has moved forward by 1.5 km in the last 5 minutes, and almost all surface flow ahead of the fire combustion is greatly perturbed by strong eddy development in the downstream flow (Figure 11b). Contrary to the CONTROL fire, which shows a decrease in the magnitude of the surface fire-induced wind speed with time, the magnitudes of the LOG surface fire-induced wind speed are increasing with time, reaching a maximum of $\sim$ 19 m s^{-1} (Figure 11c) at 600 s. Just as at 300 s, a concentrated, strong, narrow updraft begins close to the surface (Figure 11c). The black lines in Figure 11c are the 9 m s^{-1} contours for w at 100 m AGL. Although vertical motion is significant, it is found out ahead of the fire front; the maximum w at 100 m AGL was 23 m s^{-1} at (x,y) = (4.49, 1.61) km, located above the maximum convergence in the surface flow.

Although the strength of the LOG vortex couplet (Figure 11a) is slightly weaker than 5 minutes ago, it is still greater than that of the CONTROL fire (Figure 10a). The areal extent of surface flow influenced by the fire's convection column continues to grow (Figure 11c). The concave fire front tip is changed, showing an almost parabolic shape. While the strength of the fire-induced updrafts at 5 and 10 minutes in the CONTROL fire was practically the same during the same time interval, the maximum updraft speed in the LOG fire increased from 29 to 34 m s^{-1}. At 600 s into the LOG simulation, the maximum updraft speed is located at 650 m AGL, while in the CONTROL fire it is located at 1550 m, almost one kilometer higher (not shown). Even though the maximum upward velocity in the LOG fire at 600 s practically matches that in the CONTROL

fire (34 versus 33 m s^{-1}), the positioning of the maximum updraft closer to the ground appears to contribute to the LOG fire's more active surface flow features. The results suggest that a fire burning in an ambient wind with a near-surface logarithmic wind profile is capable of maintaining stronger surface fire-induced winds and vortex couplet, and a greater spread rate compared to a fire burning in an ambient wind with a constant wind profile.

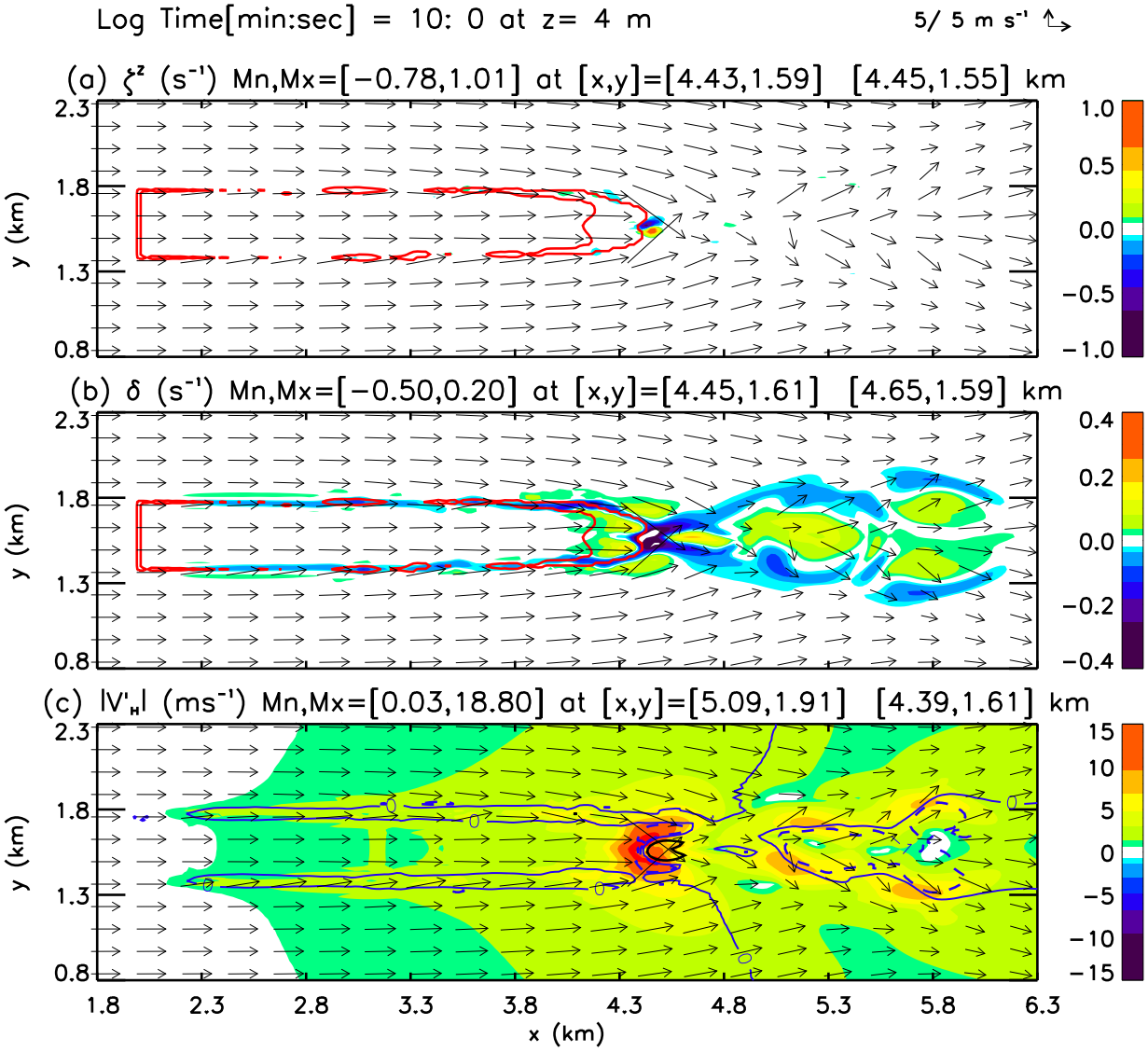

Figure 11: As in Figure 10 except for 600 s into the LOG simulation.

Figure 12 shows that there is something highly unusual about the TANH fire that cannot be seen or understood by an examination of surface flow properties only. While the CONTROL and

LOG fires have propagated by as much as 0.9 km and 1.05 km forward, respectively, in the last five minutes, the TANH fire front has moved forward by only 0.6 km. Like the LOG fire, the surface flow ahead of the fire combustion is perturbed by eddy development in the downstream flow (Figure 12b), but with disorganized patterns of weak divergence and convergence, accompanied by weak wind speed perturbations (Figure 12c). Other differences are: the diminshed vortex couplet at the head of the fire, and diminished fire-perimeter and flow-property symmetry with respect to the central east-west axis of the fire (Figure 12a); the development of concentrated but relatively weak positive/negative vertical vorticity (Figures 12a,b); and a weakly perturbed surface wind almost everywhere in the model domain (Figure 12c). The shape of the TANH fire front is no longer parabolic-like.

Two counter-rotating columns have formed roughly 300 m ahead of the fire front (Figure 12a), and their rotations are both stronger than, and opposite in sign to, the rotations in the vortex couplet at the fire's head. These vortices are accompanied by $|\vec{V}_H'|$ values of approximately 10 m s^{-1} (Figure 12c). Examination of the data shows that an additional ten-or-so weakly rotating vertical vortices formed even further downwind, and the bases of these are seen on the right in Figure 12a.

An inspection of the data indicates that the strongest TANH updraft occurs at $\approx$ 460 m AGL (not shown), lower than in the LOG or CONTROL fire plumes. The solid black lines in Figure 12c show the 5 m s^{-1} contour for w, the vertical wind component at 100 m AGL. The maximum w at 100 m AGL was 12 m s^{-1} at (x,y) = (4.75, 1.55) km, and the minimum w was -4 m s^{-1} at (x,y) = (4.63, 2.01) km. The TANH fire plume tilts significantly backward (upstream against the surface wind; not shown), and its maximum upward velocity is severely reduced compared to what it was 5 minutes ago (i.e., 18 m s^{-1} vs. 32.3 m s^{-1}), and accompanied by a substantial drop in the magnitude of the surface wind speed perturbations (Figure 12c). The disturbed flow ahead of the fire front may be partly fire-induced or partly be due to the shear-flow instability that can develop between the surface wind layer moving eastward and the upper level wind westward flow. The complex pattern of surface divergence (Figure 12b) is not present in the surface flow of the other fires. Analysis of the TANH data suggests that this pattern is associated with the existence of horizontal rolls within the first 200 m above the surface which may have been triggered by the (almost) symmetrical eddies that formed on both sides of the plume (i.e., see Figure 9b). However

Figure 12c indicates irregular surface flow throughout the fire domain, and it is not unreasonable to attribute these departures from the ambient wind to inherent instability in the background tanh wind profile (Brown, 1972).

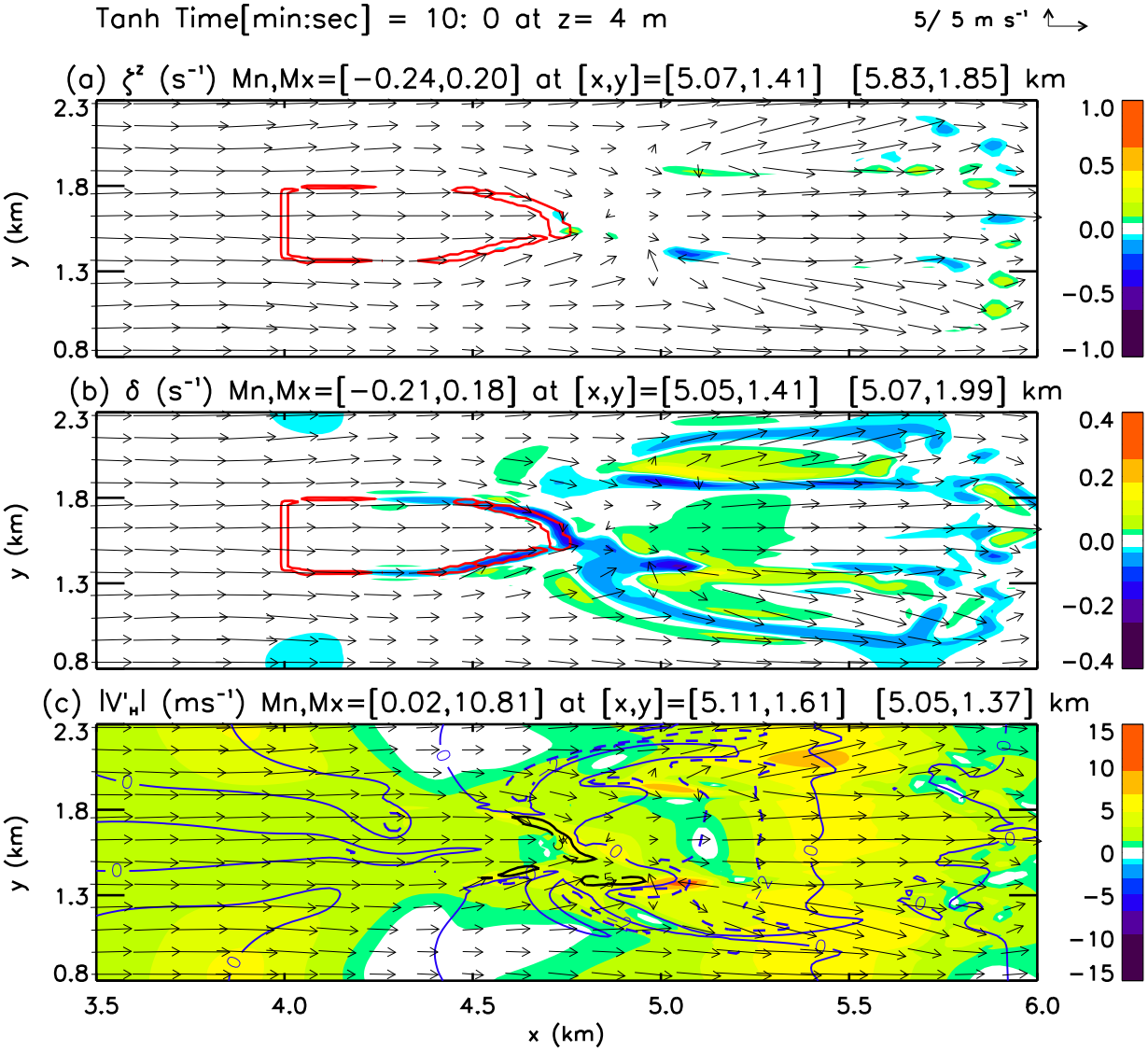

Figure 12: As in Figures 10 and 11 except for 600 s into the TANH fire simulation.

4.3 Results at 15 Minutes – End of Eastward Propagation of TANH Fire

The properties displayed in Figures 13 to 15 are the same as those displayed in Sections 4.1 and 4.2 except for 900 seconds (15 minutes) into the simulations.

The CONTROL fire at 900 s (Figure 13) shows that the near-parabolic shape of the fire front is

narrowing. The fire front has moved forward by approximately .80 km in the last 5 minutes. There are further slight decreases in the magnitudes of the surface flow properties displayed in Figure 13. Flow properties are still symmetrical with respect to the central east-west axis of the fire. The surface strength of the vortex couplet continues to decrease while the areal extent of the surface flow influenced by the fire's convection column has grown moderately (Figure 13c) over the last 5 minutes.

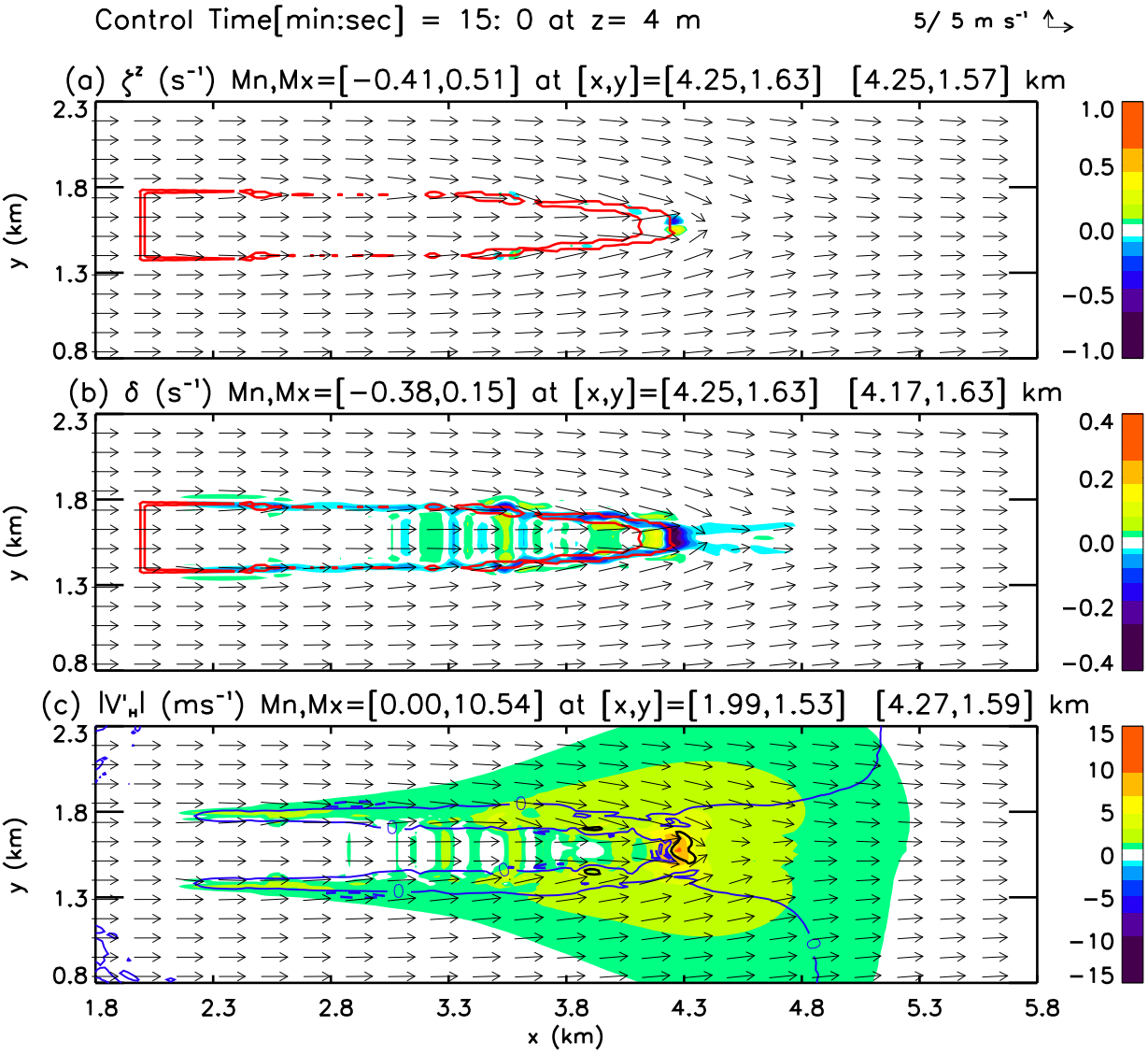

Figure 13: As in Figure 10 except for 900 seconds into the CONTROL fire simulation.

Again the magnitudes of flow properties and forward fireline propagation are slightly smaller in

the SHEAR fire (not shown) compared to the CONTROL (Figure 13). And again the only notable impact of weak negative linear vertical shear in the background wind of the SHEAR fire is to lower the forward fireline propagation.

Figure 14 shows that the LOG fire front has almost reached the east boundary of the fire domain and its propagation has slowed down somewhat; it has moved forward by 1.4 km in the last 5 minutes compared to 1.5 km in the previous 5-minute interval. The areal extent of surface flow influenced by the fire's convection column continues to grow (Figure 14c). A larger area upstream of the fire front is perturbed (Figure 14b), but the maximum wind speed perturbation is smaller than before: 6.37 m s^{-1} in Figure 14c versus 18.8 m s^{-1} in Figure 11c. The solid black lines in Figure 14c show the 7 m s^{-1} contour for w, the vertical wind component at 100 m AGL. The maximum w at 100 m AGL was 12 m s^{-1} at (x,y) = (6.13, 1.77) km, and the minimum w was -2 m s^{-1} at (x,y) = (6.13, 1.69) km. And while the strength of the vortex couplet is slightly weaker than it was 5 minutes ago, it is still greater than that of the CONTROL fire (Figure 13a). Just as for the CONTROL fire, an examination of the above-surface data shows the columns in the vortex couplet forming a V-shape in the vertical, spreading apart further with height. According to these surface properties, the LOG fire can be described as a near-steady-state but actively-moving fire; it took 15 minutes for this fire's front to travel approximately 4.5 km forward to reach the eastern edge of the fire model domain.

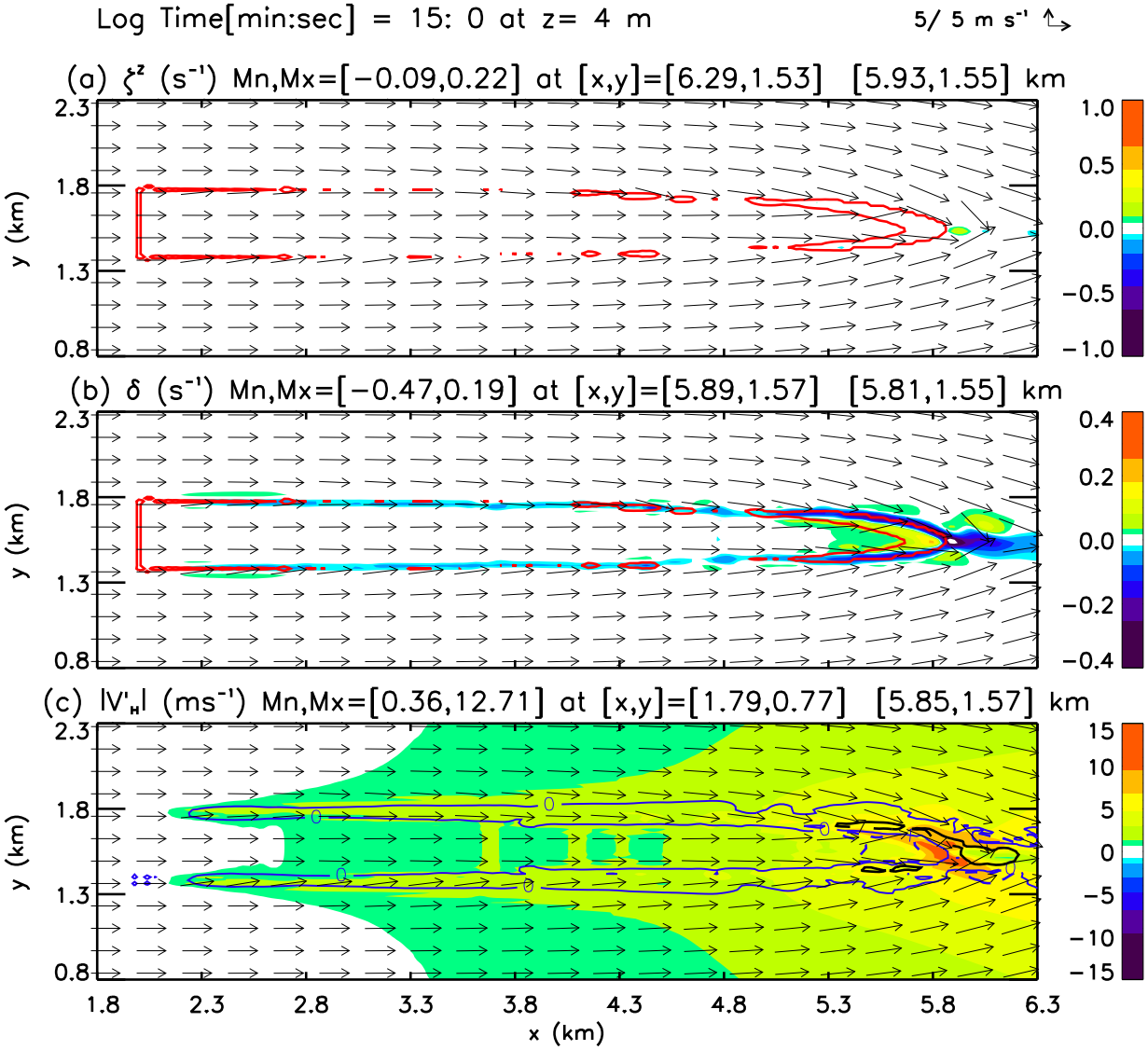

Figure 14: As in Figure 13 except for 900 s into the LOG simulation.

The TANH fire continues to behave erratically (Figure 15); any organization or symmetry in the flow patterns associated with the fire perimeter has disappeared and the fire front has effectively stopped propagating in the positive x direction. The perturbed surface horizontal wind field has strengthened, reaching maximum speeds of 14 m s^{-1} (Figure 15c), and includes multiple regions of divergence/convergence downwind of the fire (Figure 15b). Remarkably $|\vec{V}'_H|$ values are over 10 m s^{-1} on the western side ($x \leq 2.5$ km) of the fire model domain. The solid black lines in Figure 15c show the maximum w at 100 m AGL is only 8 m s^{-1} and located at (x,y) = (5.59, 1.89) km, in the upper right of the plot, a considerable distance away from the burning fire perimeter. A minimum

w of -7 m s^{-1} is located at (x,y) = (5.43, 1.87) km, nearby the maximum w in Figure 15c.

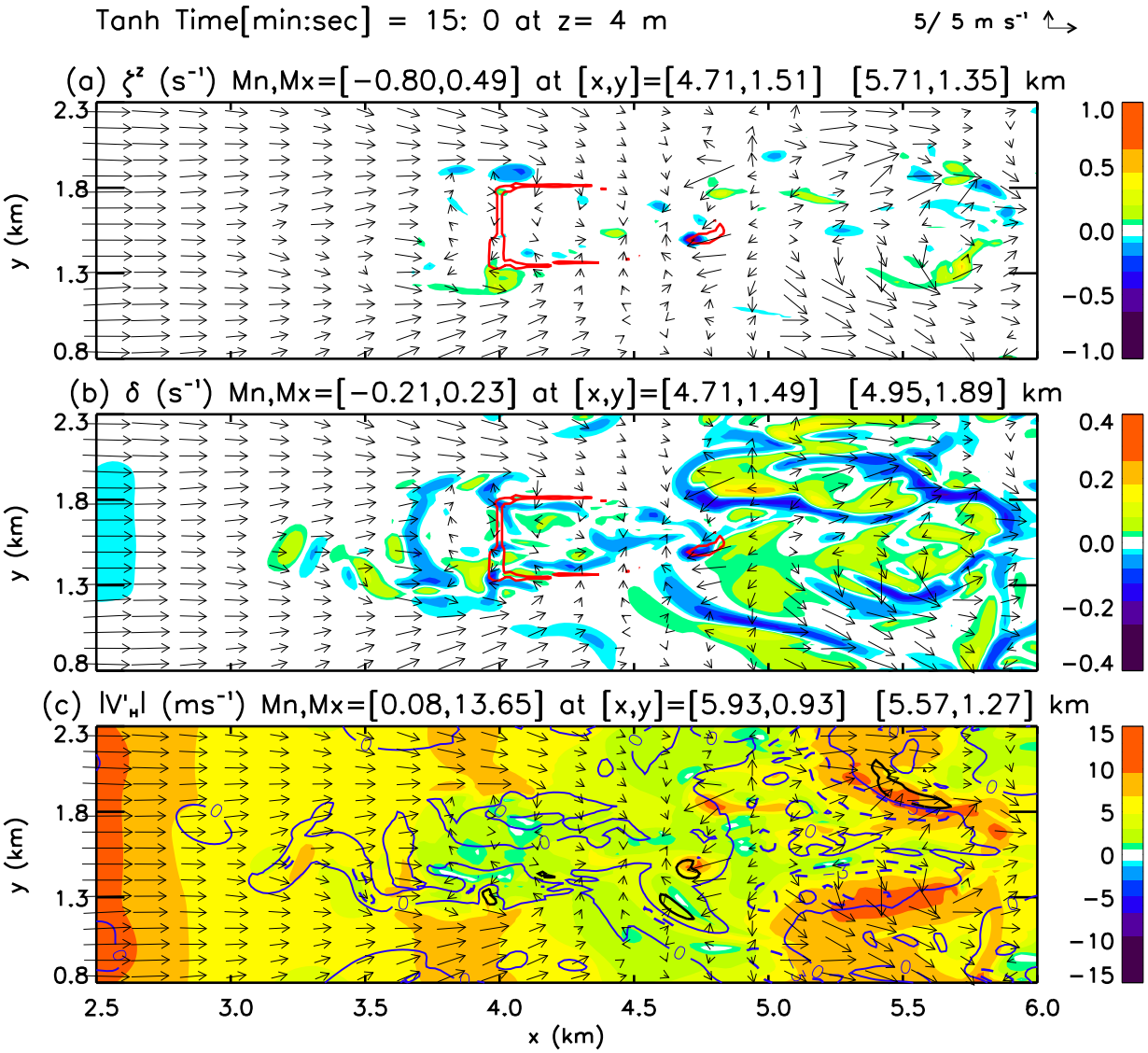

Figure 15: As in Figures 13 and 14 except for 900 s into the TANH fire simulation.

4.4 Results at 20 Minutes – Westward Propagation of TANH Fire

The properties displayed in Figures 16 and 17 are the same as those displayed in Sections 4.1 to 4.3 except for 1200 seconds (20 minutes) into the CONTROL and TANH simulations.

The CONTROL fire at 1200 s (Figure 16) shows a now narrow "pinched" fire front that has moved forward by approximately .54 km in the last 5 minutes. There are further slight decreases in the magnitudes of the surface flow properties displayed in Figure 16; flow properties are still

strongly symmetrical with respect to the central east-west axis of the fire. The vortex couplet at the fire front is not apparent in the surface flow. Examination of above-surface flow shows that the columns in the vortex couplet still exist and form a V-shape in the vertical, but no longer extend to the surface; and this vortex configuration continues until the end of the CONTROL simulation. Although convergence is still greatest at the head of the CONTROL fire, the flanks of the fire perimeter are marked by relatively moderate convergence in places (Figure 16b) along with mildly perturbed wind speeds (Figure 16c).

The results of the analyses of the SHEAR and LOG fires are not shown. Once more the magnitudes of flow properties and forward fireline propagation are slightly smaller in the SHEAR fire compared to the CONTROL (Figure 16). The fast-moving fire front of the LOG fire has exited the fire model domain; the areal extent of surface flow perturbed by the fire remains large. The most notable difference from an operational fire-fighting perspective between the behavior of the LOG fire and the CONTROL is the more rapid propagation speed of the LOG fire front downstream.

Seen first in Figure 10b in the CONTROL fire, north-south directed alternating bands of convergence/divergence in the flow inside the fire perimeter have become more numerous (Figure 16b). These bands of convergence/divergence in the surface do not appear inside the LOG fire perimeter (not shown). Examination of the model output suggests that the most likely explanation for the lack of this particular flow feature in the LOG fire is due to the strong and completely consistent forward movement of the LOG fire front; the CONTROL fire front did not move consistently forward and this appears to have affected convergence/divergence in the surface flow behind the fire front.

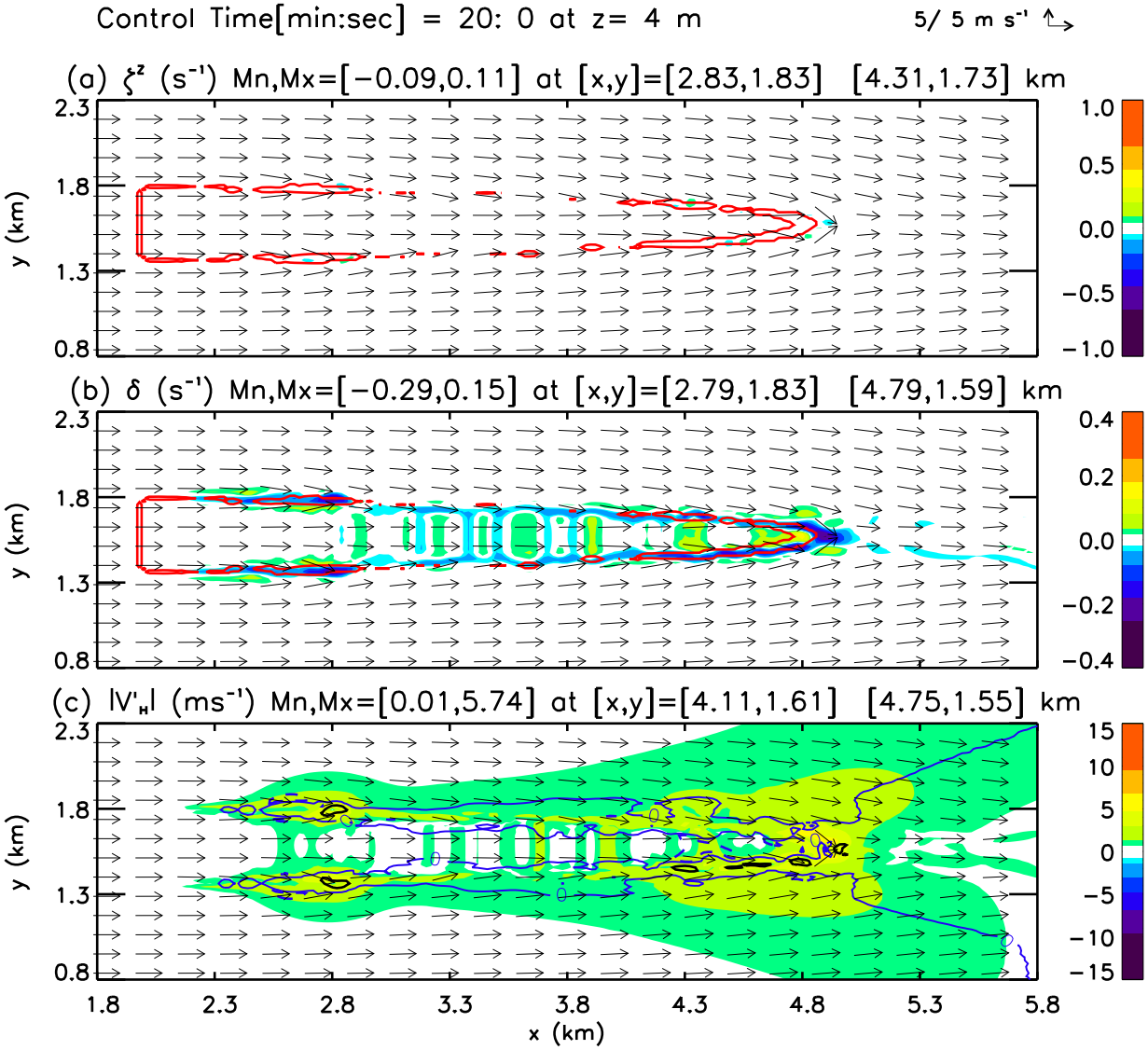

Figure 16: As in Figure 10 except for 1200 seconds into the CONTROL fire simulation.

The surface properties of TANH displayed in Figure 17 show even greater irregularity. Examination of the data shows that vertically-rotating columns (vortices) have formed almost everywhere throughout the model domain. The fire front is not propagating in the positive x direction. Animations of plots of these surface properties show several concentrated regions of negative ζ^z, with attendant regions of convergence, developing and moving in and around the western region of the TANH fire perimeter. The contours (red lines) delineating the fire perimeter in Figure 17 show this section of the fire perimeter expanding westward and southwestward. The wind vectors inside the fire perimeter show that the surface flow has reversed direction completely; they point west instead

of east. An observer on the ground would risk being buffeted by the rapidly changing winds around the TANH fire.

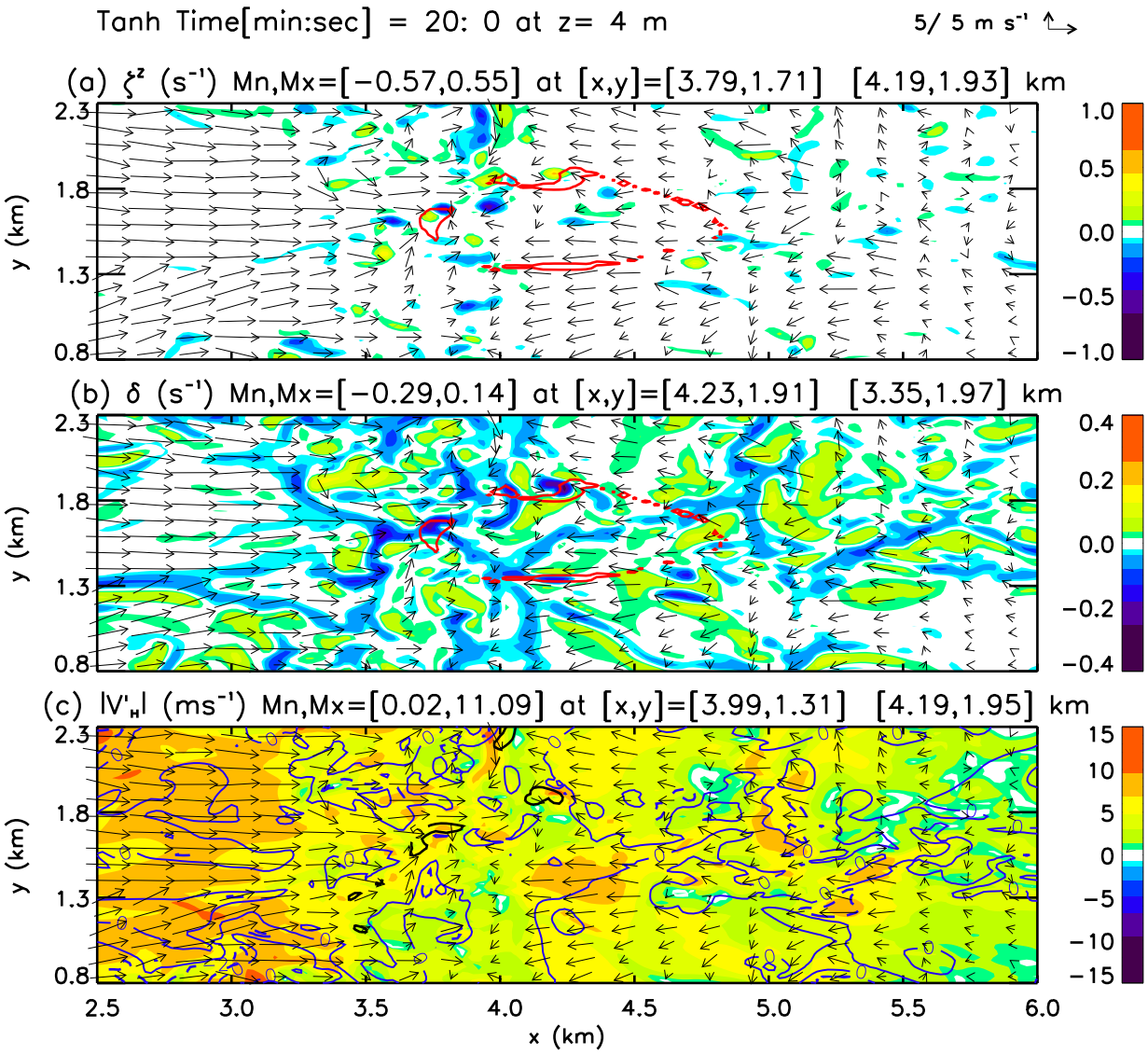

Figure 17: As in Figure 16 except for 1200 s into the TANH fire simulation.

4.5 Results at 25 Minutes – South-Westward Propagation of TANH Fire

The results displayed in Figures 18 and 19 are similar to those displayed in Sections 4.1 to 4.4 except that they are for 1500 seconds (25 minutes) into the CONTROL and TANH simulations. The analyses of the SHEAR and LOG fires are not shown. Analysis of the LOG fire shows that at this time and to the end of the simulation, forward movement of the fire front continues, with

no notable lateral expansion of the fire perimeter along the fire flanks; the original rear fireline remains intact, oriented in the north-south direction, and advances slightly westward. Again the magnitudes of flow properties and forward fireline propagation are slightly smaller in the SHEAR fire (not shown) compared to the CONTROL (Figure 18).

The CONTROL fire (Figure 18) shows an even more "pinched" fire-front shape that has moved forward by 0.54 km in the last 5 minutes. There are further slight decreases in the magnitudes of the surface flow properties displayed in Figure 18. Flow properties continue to show symmetry with respect to the central east-west axis of the fire. The base of the vortex couplet at the fire front is not apparent in Figure 18a, but the columns in the vortex couplet still exist to form a V-shape in the vertical, but no longer extend to the surface (not shown).

Although convergence is still greatest at the head of the CONTROL fire, the flanks of the fire perimeter are marked by relatively moderate convergence in places (Figure 18b) along with mildly perturbed wind speeds (Figure 18c). The regions of north-south directed alternating convergence/divergence inside the fire perimeter continue to increase in number.

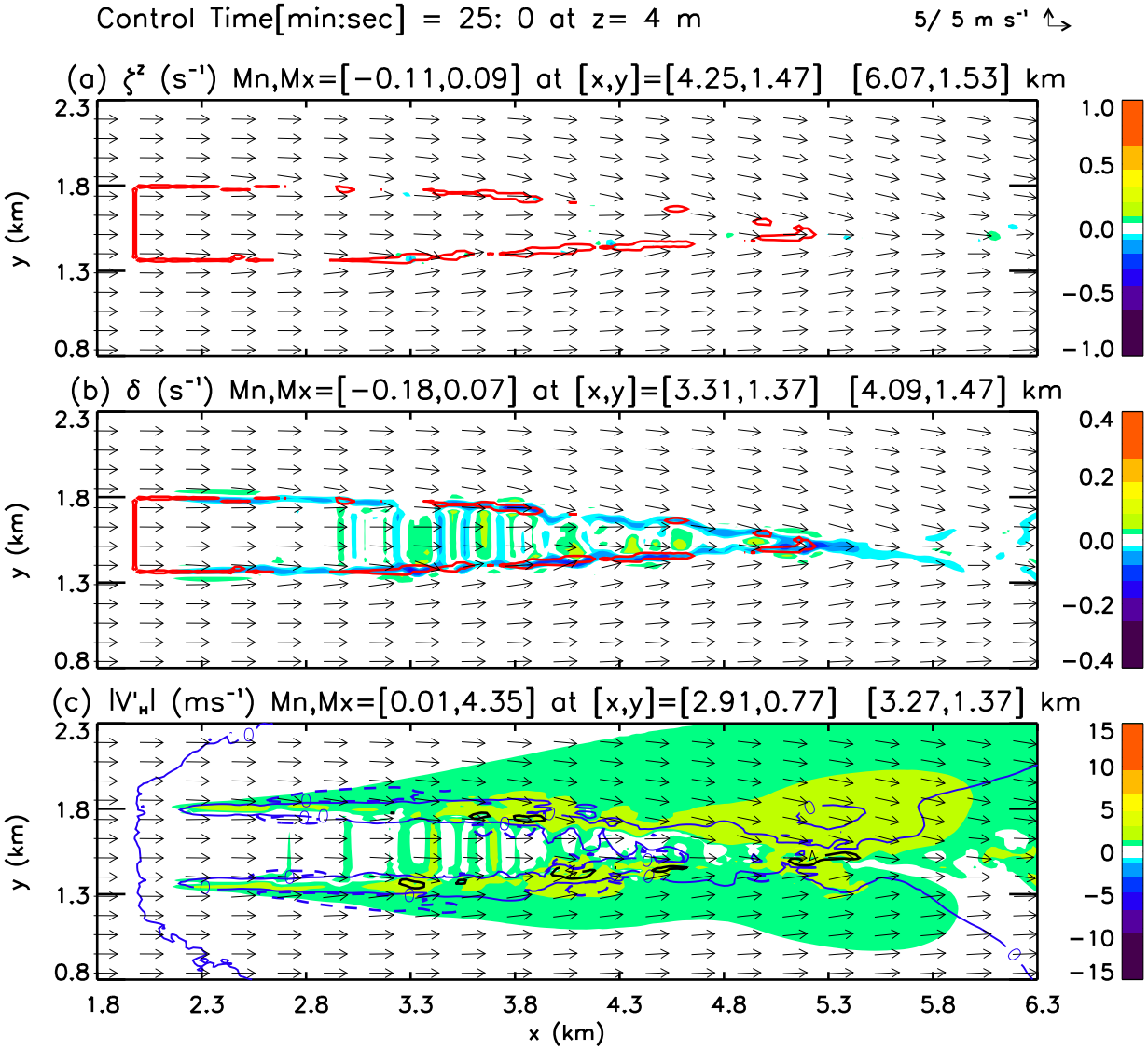

Figure 18: As in Figure 16 except for 1500 seconds into the CONTROL fire simulation.

The surface properties of TANH displayed in Figure 19 show that the TANH fire has again changed considerably in the last 5 minutes. The fire front is not propagating in the positive x direction. Vorticity activity is occuring mainly in the south-west portion of the fire perimeter (Figure 19a). Animations of plots of the surface properties show several concentrated regions of negative ζ^z, with attendant regions of convergence, developing and moving in and spiraling around the south-western region of the TANH fire perimeter. The strongest clockwise-rotating vortex (at x= 3.91 km in Figure 19a) is found near the strongest convergence (at x= 3.93 km in Figure 19b) just ahead of the strongest wind speed perturbation (at x= 3.89 km in Figure 19c) making this the

most active section of the TANH fire perimeter. Three-dimensional animations of the model data show that these multiple concentrated regions of extreme ζ^z are vertical vortices. The wind vectors show flow outside the fire's perimeter moving into the fire area, following the spiralling motion in the x-y plane induced by the vertical vortices. Figure 19c shows wind speed perturbations associated with these vertical vortices reaching 13 m s^{-1}. The red contours drawn in Figure 19 to delineate the TANH fire's perimeter show that this section of the fire perimeter has expanded south-westward, while the black contours of w at 100 m AGL in Figure 19c outline the base of the fire plume in the same location.

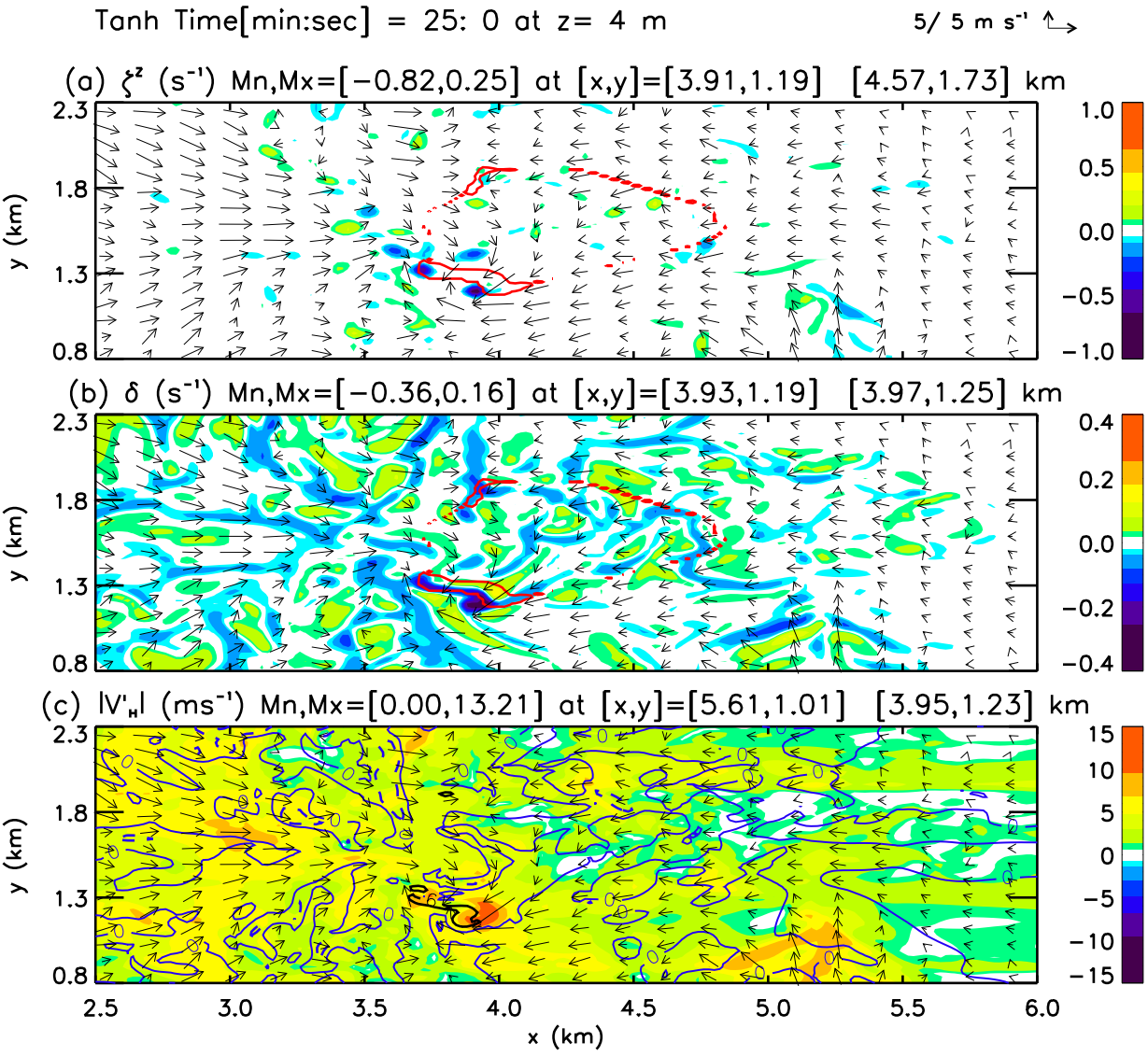

Figure 19: As in Figure 18 except for 1500 s into the TANH fire simulation.

4.6 Results at End of Simulations – Continued South-Westward Propagation of TANH Fire

The properties displayed in Figure 20 are the same as those displayed in Section 4.5 except for 1795 seconds (30 minutes) into the TANH simulation. The analyses of the CONTROL, SHEAR, and LOG fires are not shown.

There are no remarkable differences between the CONTROL fire at 1800 s compared to the CONTROL at 1500 s (Figure 18) except that there has been a slight lose of symmetry with respect to the central east-west axis of the fire, and this appears to produce very slight veering to the south-east by the CONTROL fire head.

Once more, three-dimensional animations of plots of the TANH fire show active multiple vertical vortices (Figure 20a), and those developing and moving in and spiraling around the south-western region of the TANH fire perimeter have influenced the flow to produce the change in fire perimeter seen in Figure 20. The wind speed perturbations (Figure 20a) associated with the most active and intense vertical vorticity (Figure 20a) and surface convergence (Figure 20b) reached magnitudes of 16 m s^{-1}. These flow features make the south-western region of the TANH fire perimeter the most active section of the fire. The black contour lines of w at 100 m AGL in Figure 20c show no one single well-defined base of a fire plume. The behavior of this fire and its perimeter is extremely erratic, and an observer on the ground would not necessarily be safe to have remained along the flanks or even behind the original fireline. The change from the forward-moving TANH fire at 5 minutes (Figure 6) to the fire at 30 minutes (Figure 20) is dramatic.

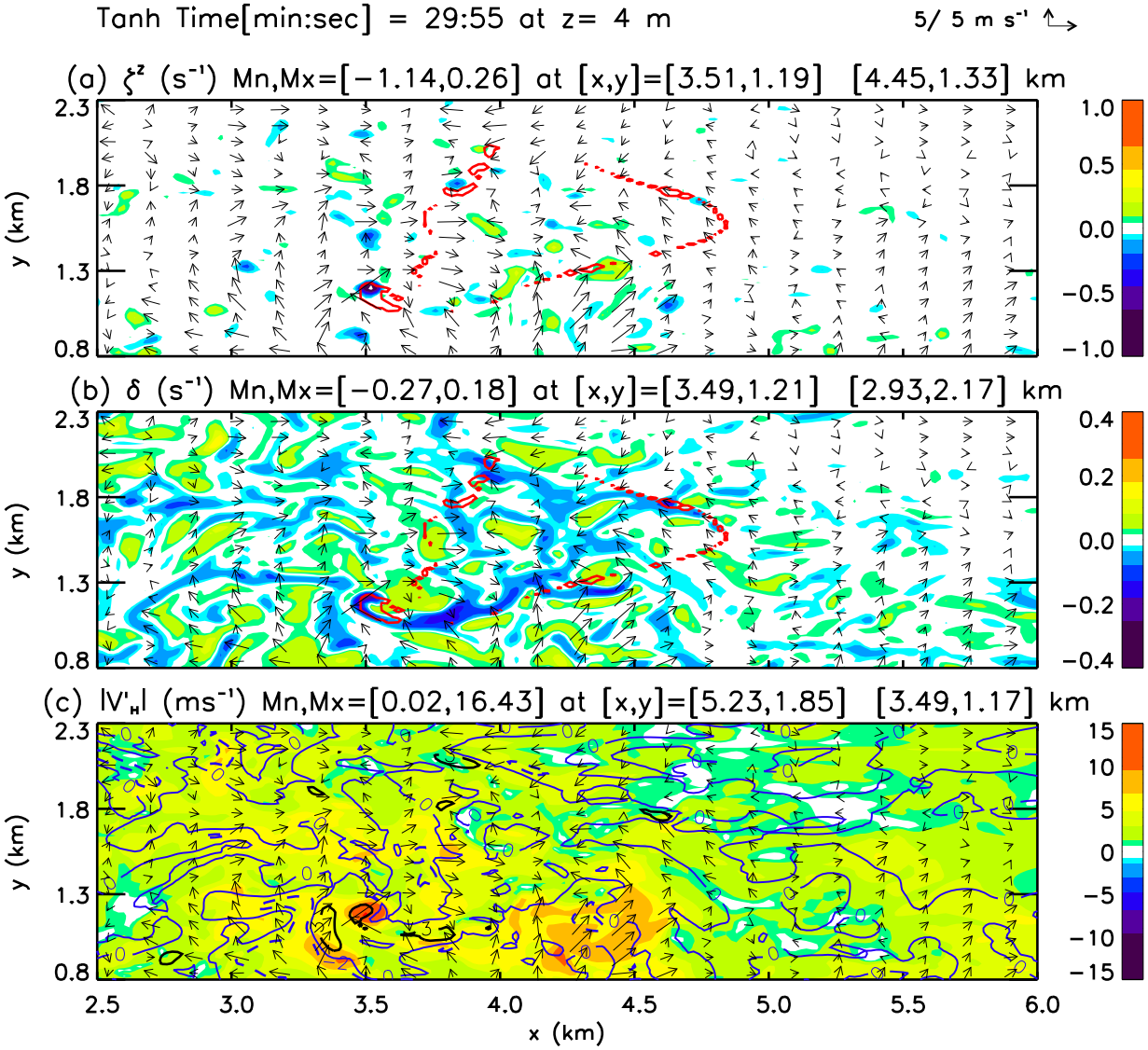

Figure 20: As in Figure 19 except for the TANH fire at 1795 s.

4.7 Burn Probability Plots

To illustrate the differences in fire spread and area burned between the four experimental fires, burn probabilities were calculated. The results for simulation times 300 s, 960 s, and 1800 s are shown, respectively, in Figures 21, 22, and 23. A 1.0 means all fires burned that area, 0.75 means three out of four fires burned that area, 0.5 means two out of four fires burned that area, and a 0.25 means one out of four fires burned that area. Since the four fires correspond to CONTROL, SHEAR, LOG, and TANH wind profiles, the red areas in Figures 21 to 23 mean that, no matter

what the background wind profile, this area will burn (100% burn probability). The other colors mean smaller probabilities. The TANH output is shifted to have the ignition line at the same location as the other simulations.

The number of numerical simulations performed were determined by computing capacity and data storage (Section 2). A sample size of four fire simulations is unquestionably small. Therefore Figures 21 to 23 do not have statistical power to estimate with confidence the uncertainty in fire spread. However they do provide evidence that there is uncertainty involved in prediction of fireline propagation and fire size, and taken together, that this uncertainty can increase in a very short time. Figure 21 shows that right at the start, in the first five minutes of the four fires, there is a significant distribution in fire spread and area burnt between the fires, even though the upstream mean surface wind was identical for the every fire.

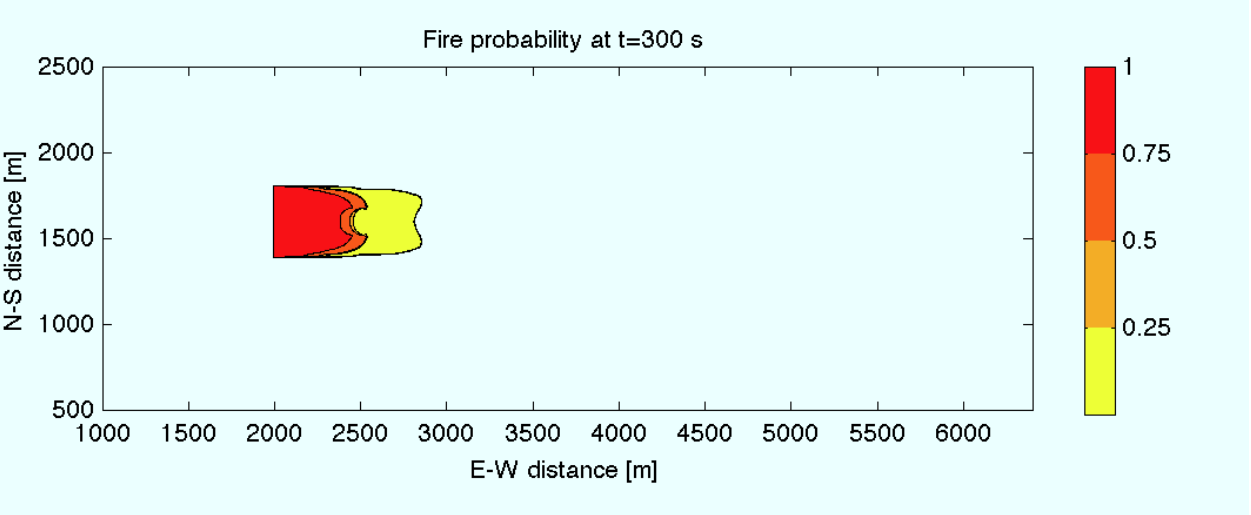

Figure 21: Burn probabilities based on the four experimental fires at 300 s (5 minutes) after fireline ignition. Initial fireline length was 400 m. See text for further explanation.

Figure 22 is the burn probability chart at 960s, and 900 to 960 s was about the time when the TANH fire stopped propagating forward (in the positive x direction). The probability map in Figure 22 shows that (in this sample) there is a chance that for 25% of these fires the backside will become the most active spread region of the fire perimeter. Figure 22 shows also that there is a chance that 25% of the fires will burn almost double the area and propagate forward by approximatively twice the distance since ignition compared to 50% of the fires.

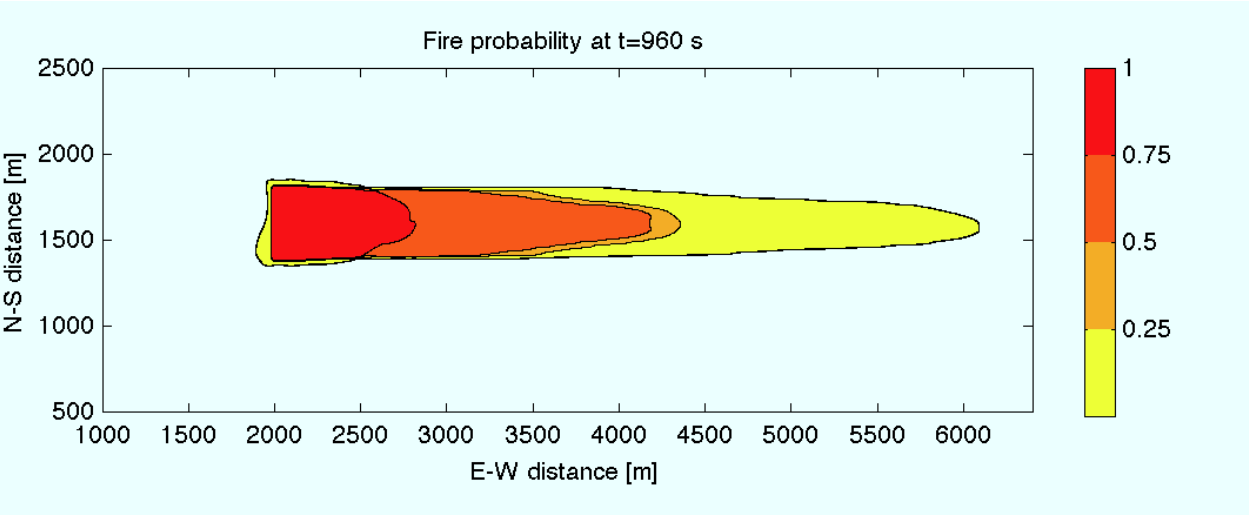

Figure 22: As in Figure 21 except for 960 s (16 minutes).

Figure 23 shows the final probability distribution of fire spread and area burnt at the end of the fire simulations. The results of this small sample are, of course, skewed by the rapid propagation of the LOG fire front through the fire model domain and by the backward movement of the TANH fire perimeter. Nonetheless, the probability distribution still serves as an illustration of the kind of variability in fire spread and area burnt that outliers can cause. Since the upstream mean surface wind was identical for the every fire, Figure 23 demonstrates that the fire-induced wind perturbations due to fire-plume/atmosphere interactions, not the upstream mean wind, are responsible for the variability in rate-of-fire-spread and area burnt. The only feature that differed between the four fires was the verical structure of the above-surface ambient wind shear, and therefore this atmospheric condition was inevitably responsible for the uncertainty in fire spread seen in Figure 23. The surface properties for the SHEAR fire were discussed previously but not shown; here Figures 21, 22, and 23 do indicate that, from an operational fire-fighting perspective, this fire, burning in an ambient wind with slightly negative linear vertical ambient wind shear, was the slowest spreading and "best behaved" fire compared to the others in the study.

The fire probability plots indicate also that the difference between the fire spread under the influence of different vertical wind shears increases substantially in time. Figure 21 analyzed alone, without knowledge of the change in burn propabilities illustrated in Figures 22 and 23, gives the (false) impression that the TANH, SHEAR and CONTROL fires will propagate in very similar way, while the LOG fire will spread much faster. Although the latter is true the former is not. The

dramatic changes from the forward-moving TANH fire at 5 minutes to what is seen at 30 minutes could not be predicted from Figure 21.

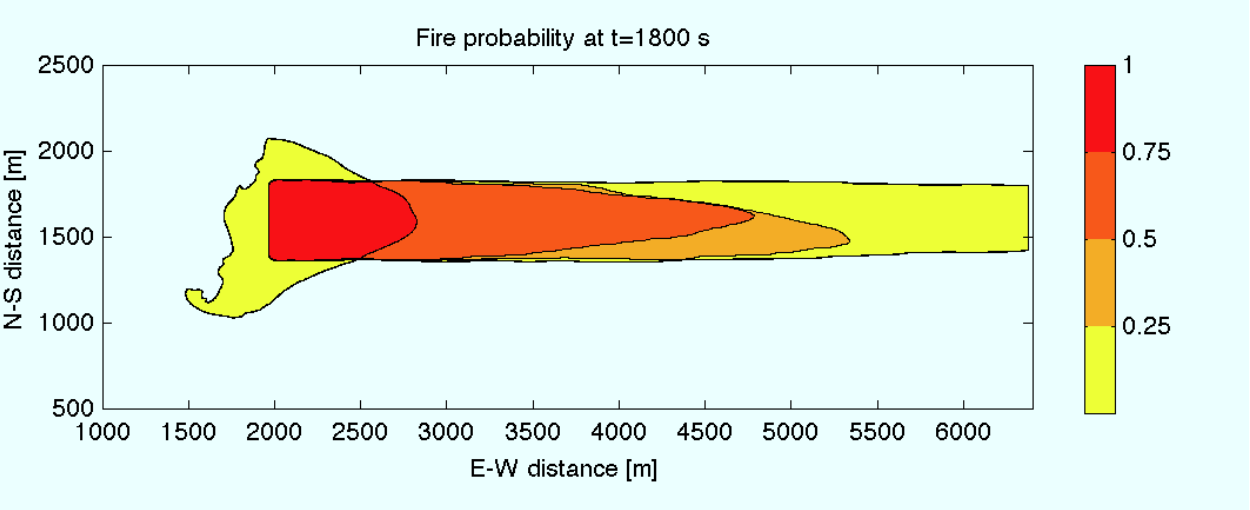

Figure 23: As in Figures 21 and 22 except for 1800 s (30 minutes).

The probability plots indicate two additional issues important to numerical fire spread prediction. The first issue is: the range of the 25% probability contour shown in Figure 23 indicates the possible error margin for predictions by current operational rate-of-fire spread models that are based solely on an estimated upstream surface wind. If fire-atmosphere coupling is not taken into account in fire spread-rate prediction, even under moderate surface wind speed conditions (5.5 m s^{-1}), the error between actual and calculated fire-front position may reach as much as 5 km within 30 minutes. The second issue is: for fire spread-rate prediction from a full-scale physically-based coupled fire/atmosphere numerical model, even small discrepancies between a forecasted and an actual wind profile may lead to serious errors in the fire spread prediction, even if the initial surface wind is forecasted correctly. Because of the uncertainty in the initial state of the atmosphere and in the numerical prediction of the evolution of coupled fire/atmosphere flow, the most useful fire-spread forecast must contain a range of predictions for the future behavior of the fire and its spread.

5 Discussion and Concluding Remarks

Fire practitioners hope that, in order to predict wildfire behavior in an operational setting, wildfire severity is dependent on a relatively small number of observable parameters defining the environments in which wildfires grow. If fireline propagation is influenced significantly by environmental characteristics, like shear in the above-surface wind, then those constitute useful observables for wildfire behavior prediction. The results of this study demonstrate that the above-surface shear in the ambient wind does impact fire propagation and behavior.

The CONTROL, SHEAR, and LOG fires can be described, from an operational point of view, as "well behaved" fires. Fire front propagation was forward and maintained a relatively consistent speed, there was no unusual activity along the flanks or rear line of the fire, and although the wind conditions in the vicinity of these fires were perturbed (especially ahead of the LOG fire front), the magnitudes of the wind fluctuations away from the fire perimeter along the flanks remained relatively low. The results imply that, in these ambient wind shear conditions, the direction and spread rate of fire-front propagation by the upstream background mean wind was not overly disrupted by fire/atmosphere-induced flow perturbations.

Although the CONTROL, SHEAR, and LOG fires did not exhibit unusual behavior throughout their lifetimes, there were significant differences in propagation speed. Depending on the vertical structure of the wind, the propagation speed of the fire front was either slower (e.g., the SHEAR fire) or faster (e.g., the LOG fire), or somewhere in between (e.g., the CONTROL fire), even though the upstream mean surface ($\leq$ 4 m AGL) wind was identical (5.5 m s^{-1}) for the grass fires.

In these fires, significant convergence in the surface was co-located with the high-speed fire-induced flow that accompanied the movement of the fire front. These findings agree generally with those of Clark et al. (1996a). However, the convergence maximum would very often lag, not lead, the fastest moving fire-induced flow. The forces responsible for the location and strength of the convergence in the surface winds that may contribute to the fronts of these fires experiencing stronger or weaker winds and propagating faster or slower were not demonstrated by the analyses. Regardless, what this study can suggest is, it is the interaction of the upper-level background wind with the fire plume, not the upstream ambient surface wind strength, that controls, indirectly, the relative position and strength of surface convergence with respect to the fire front in the CONTROL,

SHEAR, and LOG fires.

An examination of the updraft velocities in each fire plume during the stage of steady-state behavior indicates further that the magnitude of the convergence associated with the surface flow that propagates the fire front is not necessarily related directly to the strength of the fire-induced updraft. The strongest updrafts were observed in the CONTROL fire, which did not have the fastest propagating fire front. The positive vertical velocity of greatest magnitude was located significantly higher up in the CONTROL fire plume than in other experiments, which suggests that because of this, the influence of that fire's plume updraft on the surface flow was limited. Despite having the strongest vertical velocities, the surface convergence and wind speed maxima in the CONTROL fire were not as high as in the LOG fire. The LOG fire had the fastest propagating fire front. The strong near-surface vertical shear in the ambient wind field was in some way involved in the LOG updraft maximum staying closer to the surface, allowing for a greater convergence of flow into the base of the updraft. However, again, it was noted that the convergence maximum would often lag, not lead, the fastest moving fire-induced flow associated with the propagating LOG fire front.

Another feature common to all fires in this study is the existence of persistent and substantial vertical vortices. In the CONTROL, LOG, and SHEAR fires, a vortex couplet was an important feature of the fire's head. In the TANH fire, a vortex couplet was an important feature of the fire head for the first 900 seconds of the fire; after that the vortex couplet broke apart, multiple vortices developed, and the propagation of the fire became unpredictable and irregular. But regardless of the initiation, development, and behavior of these vortices in the TANH fire, many were associated with a local convergence in the surface flow, and when large enough and nearby, influenced, shaped or propagated the fire perimeter.

The TANH fire was a not "well-behaved" fire. From an operational point of view, because this fire unstable behavior, it was a dangerous fire. Fire front and fire perimeter propagation and activity were unusual and erratic; wind conditions throughout the fire model domain were perturbed, often significantly; and the largest wind speeds were associated primarily with vortex development and movement, which could be extremely irregular.

The analysis of the TANH fire suggests that fire behavior becoming dangerous or erratic can depend on environmental atmospheric conditions, and one likely condition is the structure of the vertical shear in the ambient wind field. The TANH fire simulation is a potential demonstration that

atmosphere/fire interactions are involved in "blow-up" fire behavior. As far back as Byram (1954), the forestry community suspected that a feature common to some blow-up fires is the presence of low-level negative wind shear. In the atmospheric community it is known that the mean vertical wind profile in the TANH fire is a profile inherently unstable to perturbations in the flow (Brown, 1972).

The answer to our original question, can the propagation of a wildfire be forecast accurately based on solely the strength and direction of the mean upstream near-surface wind, is therefore no it cannot. Even for identical upstream ambient surface winds, the structure of the above-surface ambient wind field and its interactions with the fire introduce uncertainty in a forecast for fire spread. Furthermore, as concluded in Sun et al. (2009), fire spread is not deterministic and a probabilistic prediction method is warranted. The results of the study support the idea that an effective operational fire-spread forecast must contain a range of predictions assessed from a statistical point of view. As for the amount of variability in fire rate-of-spread and area burnt, probability plots of the four fires in this study demonstrate that it can depend on the kind and strength of vertical shear in the ambient wind field.

In this study, the features of the surface flow involved in fire propagation are discussed without regard to the physical forces that bring about the features. An understanding of the fluid *dynamical* mechanisms involved in the influence of environmental wind shear on the evolution and propagation of wildfires would be especially valuable. This will be the focus of future research.

ACKNOWLEDGMENTS. This research was supported in part by United States Department of Agriculture Forest Service Research Joint Venture Agreement 03-JV-11231300-08, in part by Department of Commerce, National Institute of Standards and Technol ogy (NIST), Fire Research Grants Program, Grant 60NANB7D6144, and in part by a grant from the Natural Sciences and Engineering Research Council of Canada. A gratis grant of computer time from the Center for High Performance Computing, University of Utah, is gratefully acknowledged.

References

Albini, F., 1976: Estimating wildfire behavior and effects. Technical Report Report INT–30. (Ogden, UT), USDA Forest Service, Intermountain Forest and Range Experiment Station.

727 Balbi, J., J. Rossi, T. Marcelli, and P. Santoni, 2007: A 3D physical real-time model of surface
728 fires across fuel beds. *Combust. Sci. and Tech.*, **179**, 2511–2537.

729 Bluestein, H., J. LaDue, H. Stein, D. Speheger, and W. Unruh, 1993: Doppler radar wind spectra
730 of supercell tornadoes. *Mon. Wea. Rev.*, **121**, 2200–2221.

731 Brown, R., 1972: On the physical mechanism of the inflection point instability. *J. Atmos. Sci.*, **29**,
732 984–986.

733 Byram, G., 1954: Atmospheric conditions related to blowup fires. Technical Report Station Paper
734 No. 35, USDA Forest Service, Southeastern Forest Experiment Station.

735 Byram, G., 1959: *Combustion of forest fuels. In Forest Fire Control and Use. (Ed. KP Davis).*
736 McGraw Hill, New York, NY, pp 66-89 pp.

737 Cheney, P., J. Gould, and C. W.R., 1993: The influence of fuel, weather and fire shape variables
738 on fire-spread in grasslands. *International J. Wildland Fire*, **3**, 31–44.

739 Clark, T., M. Jenkins, J. Coen, and D. Packham, 1996a: A coupled atmosphere-fire model: Con-
740 vective feedback on fire–line dynamics. *J. Appl. Meteor.*, **35**, 875–901.

741 Clark, T., M. Jenkins, J. Coen, and D. Packham, 1996b: A coupled atmosphere-fire model: Role
742 of the convective froude number and dynamic fingering at the fireline. *International J. Wildland*
743 *Fire*, **6**, 177–190.

744 Forestry Canada Fire Danger Group, 1992: Development and structure of the canadian forest
745 fire behavior prediction system. Technical Report Information Report ST-X-3. (Ottawa, ON),
746 Forestry Canada.

747 Fosberg, M., and J. Deeming, 1971: Derivation of the 1- and 10-hour timelag fuel moisture
748 calculations for fire danger rating. Technical Report Research Note RM–207. (Fort Collins,
749 CO), USDA Forest Service, Rocky Mountain Forest and Range Experiment Station.

750 Houze, R., 1993: *Cloud Dynamics.* Academic Press, 573 pp, first edition.

751 Klemp, J., and D. Lilly, 1978: Numerical simulation of hydrostatic mountain waves. *J. Atmos.*
752 *Sci.*, **35**, 78–107.

753 Mandel, J., J. Beezley, L. Cobb, and A. Krishnamurthy, 2008: A wildland fire model with data
754 assimilation. *Mathematics and Computers in Simulation*, **79(3)**, 584–606.

755 Mandel, J., J. Beezley, and A. Kochanski, 2011: Coupled atmosphere-wildland fire modeling with
756 wrf 3.3 and sfire. *Geoscientific Model Development*, **4**, 1–20 doi:10.5194/gmd–4–1–2011.

757 Markowski, P., and Y. Richardson, 2010: *Mesoscale Meteorology in Midlatitudes*. Wiley-Blackwell,
758 430 pp, first edition.

759 McArthur, A., 1966: Weather and grassland fire behaviour. Technical Report Leaflet 100, Aus-
760 tralian Forestry and Timber Bureau, Canberra.

761 McArthur, A., 1967: Fire behaviour in eucalypt forest. Technical Report Leaflet 107, Australian
762 Forestry and Timber Bureau, Canberra.

763 Rothermel, R., 1972: A mathematical model for predicting fire spread in wildland fuels. Technical
764 Report Research Paper INT 115. (Ogden, UT), USDA Forest Service, Intermountain Forest and
765 Range Experiment Station, 1–46.

766 Stull, R., 1988: *An Introduction to Boundary Layer Meteorology*. Springer, 670 pp, first edition.

767 Sun, R., S. Krueger, M. Jenkins, and J. Charney, 2009: The importance of fire/atmosphere coupling
768 and boundary layer turbulence to wildfire spread. *International J. Wildland Fire*, **18**, 50–60.

769 Van Wagner, C., 1973: Height of crown scorch in forest fires. *Can. J. For. Res.*, **3**, 373–378.
770 doi:10.1139/X73–055.

771 Wang, W., Bruyère, M. Duda, J. Dudhia, H. Gill, J. Lin, J. Michalakes,
772 S. Rizvi, and X. Zhang, 2009: ARW Version 3 Modeling System User's
773 Guide. Technical report, National Center for Atmospheric Research, 310 pp.
774 [http://www.mmm.ucar.edu/wrf/users/docs/user_guide_V3/ARWUsersGuideV3.pdf].